antibiotics

MDPI

Article

Acute Intravenous Tolerability of Antimicrobial Peptides Derived from the Human Cathelicidin LL-37 and Local Antibacterial Activity of Its FK-16 Fragment in A Methicillin-Resistant *Staphylococcus epidermidis* Rat Femoral Osteotomy Model

Vincenzo Pennone [1,†], Stefania Mamberti [1,†], Giada Meogrossi [2], Monica Abbondi [2], Barbara Canciani [3], Camilla Recordati [4,5], David Sarlah [6,7,8], Fabio Sangalli [9], Elena De Vecchi [10], Emanuela Galliera [11,12] and Arianna Barbara Lovati [1,*]

[1] Cell and Tissue Engineering Laboratory, IRCCS Ospedale Galeazzi-Sant'Ambrogio, 20157 Milan, Italy; vincenzo.pennone@grupposandonato.it (V.P.); stefania.mamberti@grupposandonato.it (S.M.)
[2] Fondazione Istituto Insubrico Ricerca per la Vita, 21040 Gerenzano, Italy; giadameogrossi@ricercaperlavita.it (G.M.); monicaabbondi@ricercaperlavita.it (M.A.)
[3] Tissue Engineering and Biomaterials Laboratory, IRCCS Ospedale Galeazzi-Sant'Ambrogio, 20157 Milan, Italy; barbara.canciani@grupposandonato.it
[4] Department of Veterinary Medicine and Animal Sciences, University of Milan, 26900 Lodi, Italy; camilla.recordati@unimi.it
[5] Mouse and Animal Pathology Laboratory, UNIMI Foundation, 20139 Milano, Italy
[6] Department of Chemistry, Rice University, Houston, TX 77005, USA; sarlah@rice.edu
[7] Department of Chemistry, University of Illinois at Urbana-Champaign, Urbana, IL 61801, USA
[8] Department of Chemistry, University of Pavia, 27100 Pavia, Italy
[9] Laboratory of Medical Imaging, Department of Biomedical Engineering, IRCCS Istituto di Ricerche Farmacologiche Mario Negri, 24126 Bergamo, Italy; fabio.sangalli@marionegri.it
[10] Laboratory of Clinical Chemistry and Microbiology, IRCCS Ospedale Galeazzi-Sant'Ambrogio, 20157 Milan, Italy; elena.devecchi@grupposandonato.it
[11] Department of Biomedical Sciences for Health, University of Milan, 20133 Milan, Italy; emanuela.galliera@unimi.it
[12] Osteoimmunology Unit, IRCCS Ospedale Galeazzi-Sant'Ambrogio, 20157 Milan, Italy
* Correspondence: arianna.lovati@grupposandonato.it
† These authors contributed equally to this work.

Abstract

Background: Orthopedic implant-associated infections are difficult to eradicate because of biofilm formation and impaired healing. FK-16 and GF-17 are short synthetic antimicrobial fragments of the human cathelicidin LL-37; FK-16 consists of 16 amino acids and differs from the 17-amino-acid GF-17 by the absence of its N-terminal glycine. This study aimed to assess their acute tolerability following single-dose intravenous administration in mice and to evaluate the local antibacterial efficacy of FK-16 delivered via peptide-enriched silk fibroin (PSF) scaffolds in a rat model of methicillin-resistant *Staphylococcus epidermidis* (MRSE)-associated femoral nonunion. **Methods**: Thirty-six BALB/c mice (18 males and 18 females) received vehicle, FK-16, or GF-17 (0.1 or 1 mg/kg for each peptide) and underwent clinical and functional assessments, hemolysis testing, biochemical analyses, organ-weight measurements, and histopathological examination. Thirty-two male Wistar rats were assigned to a noninfected control group or infected groups treated with unloaded PSF, vancomycin-loaded PSF, or FK-16-loaded PSF. On day 56, antibacterial activity and bone healing were evaluated using microbiological culture, micro-computed tomography, and histopathology. **Results:** No mortality, persistent neurobehavioral

Academic Editor: Michael Samarkos

Received: 28 September 2026
Revised: 22 October 2026
Accepted: 26 October 2026
Published: 28 October 2026

Copyright: © 2026 by the author. Licensee MDPI, Basel, Switzerland. This article is an open access article distributed under the terms and conditions of the Creative Commons Attribution (CC BY) license.

abnormalities, or treatment-related organ lesions occurred in mice. Transient hind-limb paralysis occurred in one mouse treated with FK-16 and one treated with GF-17 at 1 mg/kg. Biochemical and hemolysis-related changes were isolated and did not follow a consistent dose–response pattern; no corresponding treatment-related organ lesions were observed. In rats, viable MRSE was recovered from 3/4 untreated specimens and none from those treated with vancomycin or FK-16. FK-16 was associated with partial normalization of the circulating ratio of osteoprotegerin to receptor activator of nuclear factor-κB ligand without significantly reducing early systemic inflammation. Bone mineral density, tissue mineral density, and bone volume fraction increased numerically, but no quantitative micro-computed tomography healing parameter improved significantly; the radiographic osteomyelitis score decreased significantly. Untreated PSF showed absent bridging, abundant fibrovascular tissue, chronic inflammation, rare Gram-positive cocci, and higher histological scores than noninfected controls; both treated groups showed minimal inflammation but incomplete bridging. **Conclusions:** FK-16 and GF-17 showed generally acceptable acute tolerability despite transient high-dose neurological effects. Locally delivered FK-16 demonstrated antibacterial activity, reduced osteomyelitis severity, and was associated with minimal histological evidence of inflammation, but did not significantly improve quantitative bone healing or restore complete bridging by day 56.

Keywords: antimicrobial peptides; LL-37 derivatives; silk fibroin scaffolds; implant-associated infection; methicillin-resistant *Staphylococcus epidermidis*; infected femoral nonunion

1. Introduction

Orthopedic implant-associated infections remain a major clinical burden because bacteria rapidly adhere to biomaterial surfaces and organize into biofilms, a phenotype that markedly increases tolerance to host defenses and antimicrobial therapy and can ultimately compromise fixation stability and fracture healing [1]. In particular, fracture-related infection (FRI) involving internal fixation devices is typically biofilm-associated and may progress to chronic osteomyelitis, fixation failure, and infected nonunion. Unlike periprosthetic joint infection, the management of FRI must simultaneously achieve infection control and preserve or restore the mechanical stability and biological conditions required for fracture union [2,3].

Staphylococci are major causative pathogens: in a cohort of 194 FRIs, *Staphylococcus aureus* was isolated in 31.4% of cases, *Staphylococcus epidermidis* in 25.8%, and other coagulase-negative staphylococci in 18.0%; notably, 60% of the *S. epidermidis* isolates were methicillin-resistant [4]. Biofilm formation on fixation devices, together with necrotic or poorly perfused tissue and residual dead space, contributes to bacterial persistence and impaired fracture healing. Current FRI management therefore combines adequate surgical debridement, restoration of stability, dead-space and soft-tissue management, and pathogen-directed systemic antimicrobial therapy. Local antimicrobial delivery is an adjunctive strategy intended to achieve high concentrations at the treated site and support dead-space management, rather than a replacement for surgery or systemic treatment [3].

Antimicrobial resistance further restricts treatment options for musculoskeletal infections and increases the need for alternative or adjunctive local therapies [5]. One limitation of systemic antibiotic therapy is the difficulty in achieving sustained, effective drug levels within poorly vascularized infected bone while minimizing systemic exposure; for this reason, local delivery systems and antimicrobial biomaterials have been intensively investigated in osteomyelitis and implant-related infection settings [6]. Antimicrobial peptides (AMPs), also referred to as host-defense peptides, are potential candidates for local

treatment because many exert rapid bactericidal activity and can act against planktonic and biofilm-associated bacteria. Nevertheless, bacterial adaptation to AMPs can occur. Resistance and cross-resistance to endogenous host-defense peptides may emerge, while proteolytic degradation, reduced activity in physiological fluids, limited in vivo persistence, hemolysis, and host-cell toxicity remain major barriers to clinical translation [7–9].

LL-37 is the only human cathelicidin and combines direct antimicrobial activity with immunomodulatory functions. Its antibacterial effects are mediated, at least in part, by electrostatic interactions with negatively charged bacterial membranes, leading to membrane permeabilization and bacterial killing [10,11]. GF-17 is a 17-amino-acid fragment corresponding to the major antimicrobial region of LL-37, whereas FK-16 is a 16-amino-acid fragment lacking the N-terminal glycine of GF-17. Full-length LL-37 can inhibit staphylococcal biofilm formation, whereas GF-17 has been shown to prevent bacterial attachment and disrupt established staphylococcal biofilms [12]. FK-16 has also demonstrated antibacterial activity against several antibiotic-resistant pathogens and, when immobilized on titanium surfaces, exhibits antiadhesive and biofilm-inhibitory effects [13].

However, clinical translation of AMPs, especially for indications in which systemic exposure may occur, still requires rigorous characterization of hemolytic potential, organ toxicity, and off-target host effects in vivo. In this context, FK-16 and GF-17 are LL-37–derived synthetic peptides that were previously synthesized and screened for antimicrobial performance and cytocompatibility against pathogens relevant to orthopedic infections [14].

In our previous screening of reference strains and clinical isolates relevant to orthopedic infections, FK-16 and GF-17 displayed greater anti-staphylococcal activity than full-length LL-37 and exerted bactericidal effects within preformed *S. epidermidis* biofilms, including biofilms produced by the methicillin-resistant clinical isolate used in the present study. However, their antibacterial activity was accompanied by concentration-dependent hemolytic activity and toxicity to mammalian cells, providing a direct rationale for further in vivo tolerability assessment [14]. Nevertheless, the available evidence remains largely in vitro, and in vivo data on the tolerability and local therapeutic potential of these peptides in orthopedic infections remain limited. Because systemic exposure cannot be excluded after local administration, single-dose intravenous administration was used as an acute hazard-identification approach. This experiment was not intended to reproduce the pharmacokinetic profile of scaffold implantation or to establish repeated-dose safety.

To further minimize systemic exposure while exerting local antibacterial activity, biomaterial carriers can be used to concentrate AMPs at the site of infection. Silk fibroin (SF) is an attractive matrix for bone delivery because it is biocompatible, can be processed into porous 3D scaffolds, and offers controllable degradation and opportunities for functionalization [15]. Osteoinductive peptide-enriched silk fibroin sponges (PSF) have previously been used for local vancomycin delivery in a methicillin-resistant *Staphylococcus epidermidis* (MRSE)-associated femoral nonunion model, supporting their use as a combined antimicrobial and regenerative platform [16]. During subsequent in vitro development, FK-16 was rapidly released from both SF and PSF matrices, with more than 90% released within 24 h, after which release reached a plateau; FK-16-loaded PSF also exerted bactericidal activity against MRSE. In contrast, GF-17 was released less efficiently and did not produce a significant antimicrobial effect under the same experimental conditions [17]. These peptide-specific release and efficacy data supported the selection of FK-16 over GF-17 for the local in vivo study.

Infection-associated inflammation also alters bone remodeling. Experimental staphylococcal osteomyelitis causes receptor activator of nuclear factor-κB ligand (RANKL)-dependent osteoclast formation and bone loss, indicating that antimicrobial control and modulation of bone resorption represent related but distinct biological outcomes [18,19].

Circulating osteoprotegerin (OPG) and RANKL concentrations, together with cell-count-derived inflammatory indices such as the neutrophil-to-lymphocyte ratio and systemic immune–inflammation index, were therefore included as exploratory systemic monitors. These measures were not considered substitutes for endpoints of local bacterial eradication and were interpreted together with microbiological, micro-computed tomography (micro-CT), and histopathological findings.

The aim of this study was to evaluate the acute systemic tolerability of the LL-37-derived antimicrobial peptides FK-16 and GF-17 following single-dose intravenous administration in mice and to investigate the local antibacterial efficacy of FK-16 delivered via PSF scaffolds in a rat model of MRSE-associated femoral nonunion. To address these objectives, two complementary experiments were conducted: a 24-h intravenous tolerability study in male and female BALB/c mice and a local efficacy study of FK-16-loaded PSF in rats. The intravenous experiment was designed to identify potential acute systemic adverse effects rather than to reproduce the exposure profile associated with local scaffold implantation.

The rat experiment comprised a noninfected control group (SHAM), an infected control group receiving unloaded PSF (PSF), and two infected treatment groups receiving vancomycin-loaded PSF (PSF-VANC as active comparator) or FK-16-loaded PSF (PSF-FK16). We hypothesized that local FK-16 delivery would reduce bacterial persistence, while micro-CT and radiographic outcomes were evaluated as exploratory measures of bone repair.

2. Results

2.1. Acute Intravenous Tolerability in Mice

2.1.1. Functional Observational Battery (FOB) Assessments and Survival

Formal FOB assessments performed from 15 min onward did not identify persistent neurological or autonomic abnormalities. However, during the immediate post-injection observation period, transient hind-limb paralysis occurred in 1/9 FK-16-treated and 1/9 GF-17-treated animals at 1 mg/kg. In both animals, hind-limb paralysis developed rapidly and was accompanied by an absence of response to tactile and painful stimuli. These symptoms resolved spontaneously within a few minutes, with no subsequent behavioral abnormalities observed during the remainder of the observation period (Table 1). No other abnormal clinical signs (e.g., tremors, convulsions, salivation, piloerection, or altered respiration) were observed during the scheduled assessments. Occasional minor findings, such as transient variations in activity levels or grooming, were noted in individual animals but were not dose-dependent and were considered incidental. No mortality occurred following intravenous administration of FK-16 and GF-17.

Table 1. Clinical observations and survival.

Group	Dose (mg/kg)	No. of Animals	Mortality	Clinical Signs	Time of Onset	Duration
Control	0	6	0/6	None	-	-
FK-16 low dose	0.1	6	0/6	None	-	-
FK-16 high dose	1	9	0/9	Transient hind-limb paralysis (1/9)	1–3 min	<5 min
GF-17 low dose	0.1	6	0/6	None	-	-
GF-17 high dose	1	9	0/9	Transient hind-limb paralysis (1/9)	1–3 min	<5 min

2.1.2. Body Weight

Changes in body weight were expressed as percentage changes from baseline using the formula ΔWeight% = ((final body weight − initial body weight)/initial body weight) × 100 (Table 2). No significant main effect of treatment (p = 0.281) or sex (p = 0.136) was

detected. However, a significant treatment-by-sex interaction was observed ($p = 0.017$), indicating that the effect of treatment on body weight change differed between female and male mice. Dunnett's multiple-comparisons test showed no significant differences between any treatment group and the vehicle group in female mice.

In male mice, GF-17 at a high dose resulted in a significantly lower percentage body weight change than vehicle treatment ($p < 0.01$). No other treatment group differed significantly from the corresponding vehicle group. Separate Kruskal–Wallis sensitivity analyses did not identify significant treatment differences in either female mice ($p = 0.094$) or male mice ($p = 0.162$). Therefore, the significant reduction observed in male mice treated with GF-17 at a high dose should be interpreted cautiously because of the small sample size and the high proportion of unchanged body weight values.

Table 2. 24-h percentage change in body weight (%, mean ± SEM).

Group	Male	Female
Control	3.33 ± 3.33 (n = 3)	−0.90 ± 0.90 (n = 3)
FK-16 low dose	1.59 ± 1.59 (n = 3)	−4.23 ± 2.16 (n = 3)
FK-16 high dose	0.00 ± 0.00 (n = 5)	0.00 ± 0.00 (n = 4)
GF-17 low dose	1.75 ± 1.75 (n = 3)	0.00 ± 0.00 (n = 3)
GF-17 high dose	−3.75 ± 2.39 ** (n = 4)	0.62 ± 0.62 (n = 5)

** $p < 0.01$, significant vs. control.

2.1.3. Hemolysis-Associated Plasma Absorbance

Hemolysis was evaluated by spectrophotometric measurement of plasma absorbance at 540 nm, indicative of free hemoglobin, at 3 h and 24 h following intravenous administration of FK-16 or GF-17 (Table 3). A three-way repeated-measures analysis of variance (ANOVA) revealed a significant main effect of treatment on absorbance at 540 nm ($p < 0.0001$). A significant treatment-by-sex interaction was also observed ($p = 0.002$), indicating that the effect of treatment differed between male and female mice. No significant main effect of sex was detected ($p = 0.157$), and absorbance values did not show a significant overall change between 3 and 24 h ($p = 0.263$). No significant treatment-by-time ($p = 0.967$), sex-by-time ($p = 0.376$), or treatment-by-sex-by-time ($p = 0.156$) interactions were observed. The multiple-comparisons test showed that, in male mice at 24 h, treatment with FK-16 at a low dose significantly increased absorbance compared with the vehicle group ($p = 0.0205$). No other treatment group differed significantly from its corresponding vehicle group in either male or female mice at 3 or 24 h. Furthermore, no significant differences between the 3- and 24-h measurements were detected within any treatment and sex group.

Table 3. Hemolysis-associated absorbance at 540 nm following in vivo administration of FK-16 or GF-17 (mean ± SEM).

	Female		Male	
Group	**3 h**	**24 h**	**3 h**	**24 h**
Control	0.26 ± 0.07 (n = 3)	0.23 ± 0.16 (n = 3)	0.16 ± 0.05 (n = 3)	0.10 ± 0.08 (n = 3)
FK-16 low dose	0.14 ± 0.03 (n = 3)	0.06 ± 0.06 (n = 3)	0.25 ± 0.08 (n = 3)	0.35 ± 0.04 * (n = 3)
FK-16 high dose	0.13 ± 0.01 (n = 4)	0.25 ± 0.10 (n = 4)	0.35 ± 0.12 (n = 5)	0.15 ± 0.14 (n = 5)
GF-17 low dose	0.06 ± 0.00 (n = 3)	0.04 ± 0.03 (n = 3)	0.14 ± 0.06 (n = 3)	0.04 ± 0.03 (n = 3)
GF-17 high dose	0.11 ± 0.02 (n = 5)	0.09 ± 0.07 (n = 5)	0.10 ± 0.04 (n = 4)	0.04 ± 0.01 (n = 4)

* $p < 0.05$, significant vs. control.

2.1.4. Biochemical Analysis

One sample from a control male was excluded from the analysis because of insufficient sample material. Analysis of biochemical parameters revealed significant treatment effects on alanine aminotransferase (ALT) activity and total bile acids (both $p < 0.0001$), as well as on aspartate aminotransferase (AST) activity and creatinine (both $p < 0.05$). No significant effects of sex or treatment-by-sex interactions were found (Table 4). ALT activity was lower in both GF-17 groups than in controls ($p < 0.0001$). AST did not differ significantly among groups. Creatinine was higher in the GF-17 low-dose group than in controls ($p < 0.05$). However, absolute creatinine concentrations were unexpectedly elevated in all groups, including controls, relative to standard values for healthy mice. Because we could not exclude possible analytical bias and independent confirmatory measurements were unavailable, we did not use creatinine values to infer renal function, and we interpreted the observed between-group difference cautiously. Total bile acids were lower in the FK-16 high-dose group than in controls ($p < 0.0001$). Overall, these biochemical changes did not follow a consistent dose–response pattern and were not accompanied by treatment-related hepatic or renal histopathological lesions.

Table 4. Biochemical parameters (mean ± SEM).

Parameter	Control	FK-16 Low Dose	FK-16 High Dose	GF-17 Low Dose	GF-17 High Dose
ALT (U/L)	80.94 ± 1.77	85.59 ± 5.12	82.71 ± 0.68	39.15 ± 0.68 ****	45.19 ± 2.16 ****
AST (U/L)	26.27 ± 2.78	33.08 ± 4.73	43.48 ± 2.32	22.85 ± 4.68	30.53 ± 6.09
Creatinine (µmol/L)	124.31 ± 5.51	156.70 ± 4.84	134.77 ± 4.47	160.10 ± 13.82 *	146.66 ± 8.35
Total bile acids (µmol/L)	2.09 ± 0.19	2.64 ± 0.20	0.88 ± 0.03 ****	2.12 ± 0.31	1.86 ± 0.21

**** $p < 0.0001$; * $p < 0.05$, significant vs. control. Absolute creatinine concentrations were unexpectedly elevated in all groups and may reflect analytical bias. These values should not be used to infer renal function, and between-group differences should be interpreted cautiously.

2.1.5. Gross Necropsy and Relative Organ Weights

The liver, thymus, kidneys, and spleen were dissected and weighed; macroscopic examination revealed no abnormalities. Relative organ weights were calculated as follows: [organ weight (g)/body weight (g)] × 100; for the kidneys, the combined weight of both kidneys was used (Table 5). The two-way ANOVA identified a significant main effect of sex for spleen and thymus ($p < 0.001$), kidneys ($p = 0.003$), and liver ($p < 0.01$). The main effect of treatment was significant for the liver ($p < 0.01$) and thymus ($p < 0.02$), and the sex × treatment interaction was significant for the kidneys ($p = 0.027$); no other treatment-related main effects or interactions were significant. Overall, these differences were more consistent with physiological sex-related variation than with peptide administration. For the kidneys, subsequent analyses performed separately in males and females did not identify significant treatment-related differences. Moreover, the group variations did not follow a consistent dose–response pattern. Therefore, the interaction was not considered indicative of a treatment-related adverse effect. For the liver, post hoc comparisons identified a difference between the FK-16 high-dose and GF-17 low-dose groups ($p < 0.01$); however, neither group differed significantly from the control group. Given the absence of a consistent dose–response relationship or treatment-related macroscopic findings, this isolated difference was considered incidental and not toxicologically relevant. For the thymus, post hoc comparisons showed higher relative thymus weights in the FK-16 high-dose and GF-17 low-dose groups compared with controls (both $p < 0.05$). Nevertheless, these findings were not associated with a consistent dose–response relationship and were not supported by macroscopic or histopathological alterations. Accordingly, they were not considered adverse or toxicologically relevant.

Table 5. Relative organ weights (% of body weight; mean ± SEM).

	Male					Female			
Group	**n**	**Spleen**	**Kidneys**	**Liver**	**Thymus**	**n**	**Spleen**	**Kidneys**	**Liver**	**Thymus**
Control	3	0.50 ± 0.01	1.89 ± 0.04	6.26 ± 0.16	0.33 ± 0.04	3	0.59 ± 0.05	1.42 ± 0.06	5.75 ± 0.14	0.42 ± 0.05
FK-16 low dose	3	0.50 ± 0.02	1.55 ± 0.18	5.69 ± 0.28	0.37 ± 0.03	3	0.62 ± 0.04	1.86 ± 0.37	5.58 ± 0.15	0.51 ± 0.02
FK-16 high dose	5	0.50 ± 0.01	1.78 ± 0.03	5.72 ± 0.18	0.42 ± 0.03 *	4	0.53 ± 0.02	1.44 ± 0.03	5.27 ± 0.15	0.56 ± 0.03 *
GF-17 low dose	3	0.52 ± 0.04	1.74 ± 0.05	6.51 ± 0.26	0.50 ± 0.06 *	3	0.59 ± 0.01	1.41 ± 0.06	6.04 ± 0.38	0.51 ± 0.02 *
GF-17 high dose	4	0.53 ± 0.01	1.79 ± 0.02	6.33 ± 0.18	0.41 ± 0.04	5	0.59 ± 0.04	1.48 ± 0.02	5.64 ± 0.09	0.50 ± 0.02

* $p < 0.05$, significant vs. control.

2.1.6. Histopathological Findings

No microscopic findings were considered treatment-related. The spleen and thymus were histologically unremarkable in all animals, and no microscopic alterations were recorded in the majority of liver and kidney specimens. Focal mononuclear cell infiltrates were observed in the liver of seven mice. A minimal focal infiltrate was present in one vehicle-control animal (1/6). In contrast, minimal focal infiltrates were observed in one animal receiving FK-16 at 0.1 mg/kg (1/6), three animals receiving FK-16 at 1 mg/kg (3/9), one animal receiving GF-17 at 0.1 mg/kg (1/6), and one animal receiving GF-17 at 1 mg/kg (1/9). Minimal focal tubular basophilia was observed in the kidney of one mouse receiving FK-16 at 0.1 mg/kg (1/6) and was not detected in the remaining animals. The hepatic infiltrates and the isolated renal finding were of low severity, were focal in distribution, occurred across control and treated groups, and showed no consistent dose-related pattern. On this basis, they were considered incidental background alterations rather than treatment-related lesions. No other microscopic abnormalities were recorded in the organs examined.

2.2. Local Antibacterial Efficacy in A Rat Model of Implant-Related Bone Infection

2.2.1. Animal Flow, Clinical Observations, and Postoperative Course

All 32 rats completed the 56-day follow-up and underwent euthanasia. One animal in the SHAM group had an uneventful postoperative course, with no local swelling, impaired weight bearing, or lameness throughout the observation period. Loss of fixation integrity was identified only during postmortem micro-CT examination of the explanted femur and had not been clinically apparent during follow-up. Because the resulting mechanical instability invalidated evaluation of the standardized osteotomy model, this specimen was excluded from the micro-CT and histopathological analyses. The animal remained included in longitudinal clinical, body-weight, and blood-based analyses. No other fixation failures or serious adverse events were identified. Surgical wounds remained closed and showed normal postoperative healing, with no wound dehiscence, purulent discharge, persistent exudate, or other overt local signs of infection. Mild localized swelling around the operated limb was occasionally observed in individual animals during the postoperative period. This finding was transient and was not associated with wound complications, impaired mobility, reduced weight bearing, or signs of systemic illness. No consistent difference in the occurrence or severity of swelling was apparent among the experimental groups. Animals remained mobile and were able to bear weight on the operated limb throughout follow-up. No persistent lameness, abnormal behavior, or signs of clinically relevant distress were recorded. Routine perioperative analgesia was considered sufficient, and no additional rescue analgesia was required. Overall, the surgical procedure and local scaffold treatments were clinically well tolerated under the conditions of the study.

2.2.2. Body Weight

Body weight was monitored over 56 days to evaluate the systemic impact of infection and treatment. All groups exhibited a progressive increase in body weight over time. Body-weight changes were expressed as the percentage change from each animal's baseline value on day 0. On day 56, body-weight increases were 26.75 ± 5.01%, 26.72 ± 2.50%, 22.22 ± 4.13%, and 19.32 ± 3.28% in the SHAM, PSF, PSF-VANC, and PSF-FK16 groups, respectively. The increase was lower in the PSF-VANC group than in the PSF group ($p < 0.05$) and lower in the PSF-FK16 group than in the PSF group ($p < 0.001$). No statistically significant differences were observed between the SHAM and PSF groups at any evaluated time point, including day 56 (Figure 1).

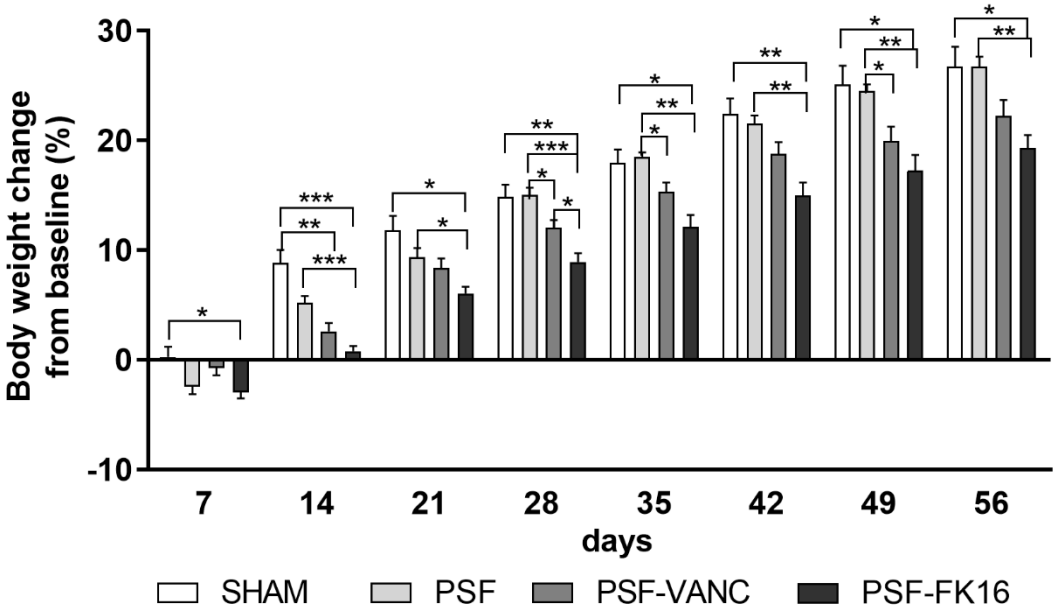


Figure 1. Changes in body weight during the experimental period. Data are presented as mean ± SEM (n = 8 per group). Statistically significant comparisons are shown: * $p < 0.05$, ** $p < 0.01$, and *** $p < 0.001$.

2.2.3. Assessment of Systemic Inflammation Following MRSE Infection and Treatment

Circulating neutrophil counts, the neutrophil-to-lymphocyte ratio (NLR), and the Systemic Immune–Inflammation Index (SII) were assessed over time to characterize the systemic inflammatory response following MRSE infection and treatment (Figure 2). On day 7, the PSF group showed significantly higher neutrophil counts than the SHAM group ($p < 0.05$), together with higher NLR and SII values (both $p < 0.001$). Compared with PSF, PSF-VANC showed significantly lower neutrophil counts ($p < 0.01$), NLR ($p < 0.01$), and SII ($p < 0.01$), indicating attenuation of the day-7 inflammatory response. A small number of measurements were unavailable because of pre-analytical issues (e.g., insufficient sample volume or clotting) or invalid instrument results. These measurements were treated as missing data, resulting in variable sample sizes across groups and time points. No statistically significant pairwise comparisons involving the PSF-FK16 group were detected at this time point. No significant between-group differences were observed on days 28 or 56. Overall, these findings indicate a transient systemic inflammatory response in the PSF group on day 7 that was significantly attenuated by vancomycin treatment.

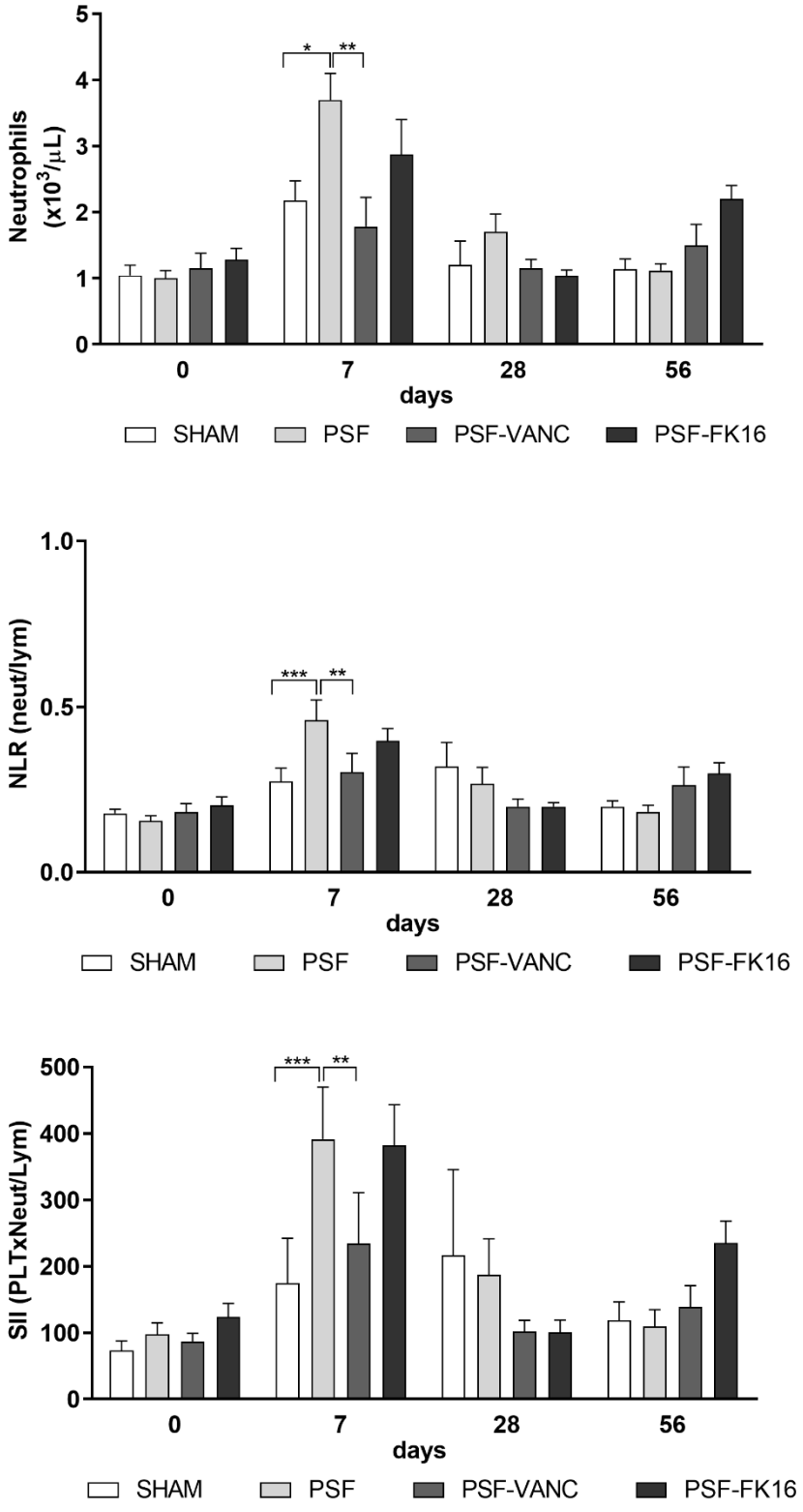


Figure 2. Changes in circulating neutrophils, neutrophil-to-lymphocyte ratio (NLR), and systemic immune-inflammation index (SII) following MRSE infection and treatment. NLR, neutrophil-to-lymphocyte ratio; SII, platelet count × neutrophil count/lymphocyte count. Data are presented as mean ± SEM. Statistically significant comparisons: * $p < 0.05$, ** $p < 0.01$, and *** $p < 0.001$.

2.2.4. Modulation of the OPG/RANKL Osteoimmunological Axis

Serum OPG and RANKL concentrations and the corresponding OPG/RANKL ratio were evaluated to investigate the effects of MRSE infection and local antimicrobial

treatments on systemic regulators of bone remodeling (Figure 3). At baseline, serum OPG concentrations were comparable among groups, indicating similar preoperative conditions. On day 2, OPG was significantly lower in the infected PSF group than in SHAM animals ($p < 0.05$). Both antimicrobial treatments counteracted this early reduction, with significantly higher OPG concentrations in PSF-VANC and PSF-FK16 animals than in the untreated PSF group ($p < 0.05$ and $p < 0.01$, respectively). Additional between-group differences emerged on day 28. OPG concentrations were markedly lower in the PSF group than in SHAM animals ($p < 0.0001$). Both PSF-VANC and PSF-FK16 significantly increased circulating OPG compared with PSF animals ($p < 0.0001$ and $p < 0.001$, respectively). On day 56, OPG remained significantly lower in the PSF group than in SHAM animals ($p < 0.01$). OPG concentrations were also significantly higher in both PSF-VANC and PSF-FK16 animals than in the PSF group ($p < 0.01$ and $p < 0.001$, respectively). Although the PSF-FK16 group had the highest mean OPG concentration at the final time point, it did not differ significantly from either the SHAM or PSF-VANC group. Overall, untreated infection (PSF) was associated with persistently lower circulating OPG, whereas both local antimicrobial treatments preserved or restored OPG concentrations. RANKL concentrations were comparable among groups at baseline and at day 2. On day 28, RANKL was significantly higher in the infected PSF group than in SHAM animals ($p < 0.05$). Vancomycin treatment significantly reduced RANKL compared with PSF animals ($p < 0.05$), whereas no significant difference was observed between PSF-FK16 and PSF at this time point. On day 56, RANKL remained significantly elevated in the PSF group compared with SHAM animals ($p < 0.001$). Both PSF-VANC and PSF-FK16 significantly reduced circulating RANKL relative to the untreated PSF group ($p < 0.01$ and $p < 0.001$, respectively). These findings indicate that untreated MRSE infection (PSF group) was associated with a sustained increase in systemic pro-osteoclastogenic signaling, whereas both antimicrobial treatments attenuated the late RANKL response. The OPG/RANKL ratio did not differ among groups at baseline. At day 2, the ratio was significantly lower in the PSF group than in SHAM animals ($p < 0.05$), indicating an early infection-associated shift toward a more pro-osteoclastogenic systemic environment. Both PSF-VANC and PSF-FK16 significantly increased the ratio compared with PSF animals ($p < 0.05$ and $p < 0.01$, respectively). Significant differences persisted at the later time points. On day 28, the OPG/RANKL ratio was lower in the PSF group than in SHAM animals ($p < 0.01$). Both PSF-VANC and PSF-FK16 significantly increased the ratio compared with PSF ($p < 0.01$ and $p < 0.05$, respectively). Similarly, on day 56, the ratio was markedly lower in PSF animals than in SHAM animals ($p < 0.0001$), whereas both PSF-VANC and PSF-FK16 produced significantly higher ratios than untreated PSF ($p < 0.01$ for both comparisons).

https://doi.org/10.3390/antibiotics15111077

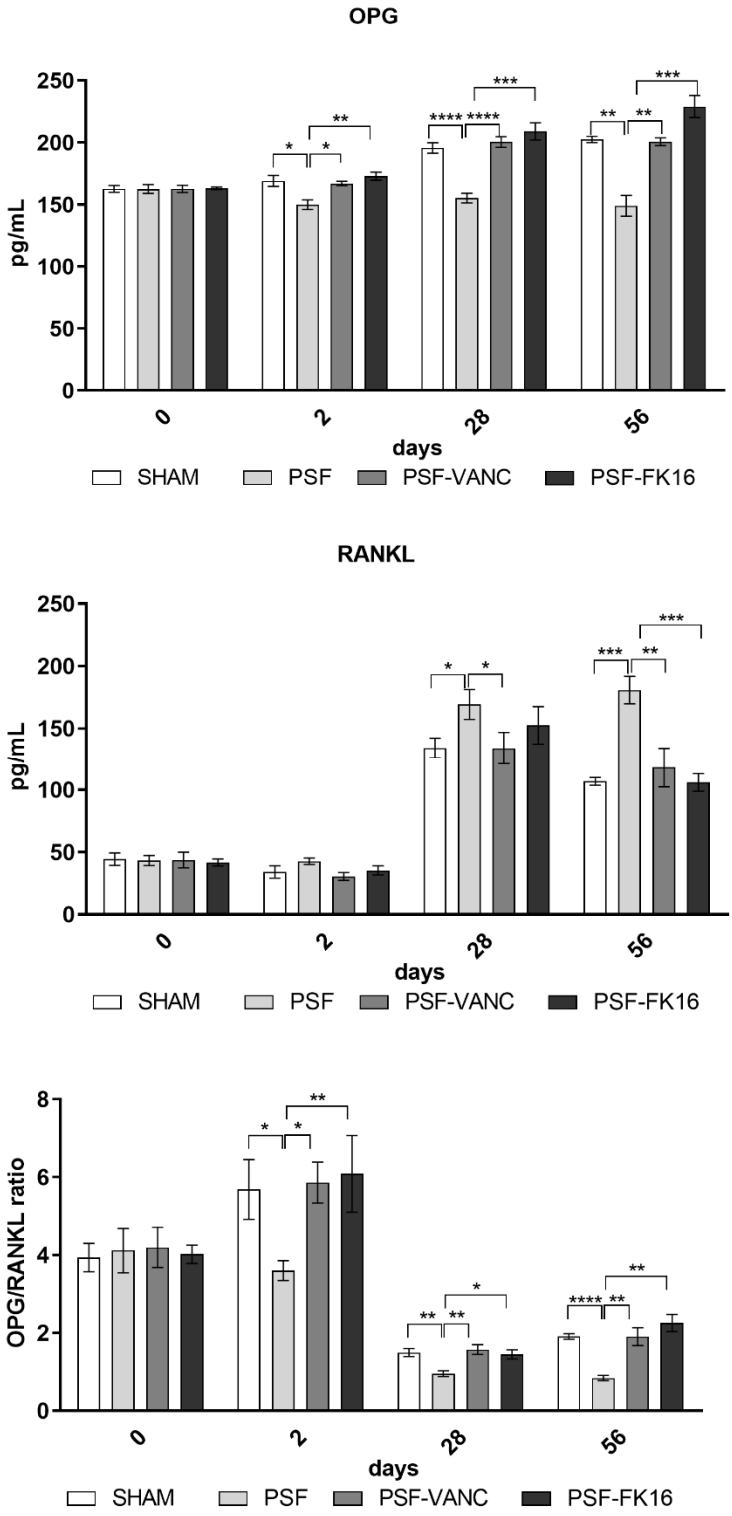


Figure 3. Evaluation of circulating OPG, RANKL, and the OPG/RANKL ratio. Serum osteoprotegerin (OPG), receptor activator of nuclear factor-κB ligand (RANKL), and the corresponding OPG/RANKL ratio were assessed at baseline and on days 2, 28, and 56. Data are expressed as mean ± SEM (n = 8 per group). Statistical significance is indicated as * $p < 0.05$, ** $p < 0.01$, *** $p < 0.001$, and **** $p < 0.0001$.

2.2.5. Microbiological Results

On day 56, following euthanasia, four specimens per group were collected for microbiological analysis (n = 4 per group). On tryptic soy agar (TSA), bacterial growth was detected in PSF specimens (3/4), with counts ranging from 33.3 to 2.11 × 10^3 CFU/mL. On mannitol salt agar (MSA), bacterial growth was detected in the same PSF specimens, with counts ranging from 33.3 to 1.79 × 10^3 CFU/mL. No growth was detected in the SHAM, PSF-VANC, or PSF-FK16 groups (0/4 each) by the methods used. Bacterial-count data were primarily interpreted descriptively.

2.2.6. Micro-CT Results

On day 56, micro-CT analysis was performed to quantify bone mineralization and microarchitecture within the femoral defect (Figure 4). Seven SHAM specimens and eight specimens from each infected group were included. One SHAM dataset was excluded because postmortem micro-CT examination revealed loss of fixation integrity. The infected PSF group showed significantly lower values than the SHAM group for bone mineral density (BMD, $p < 0.05$), tissue mineral density (TMD, $p < 0.01$), and bone volume fraction (BV/TV, $p < 0.05$). These findings indicate that MRSE infection adversely affected bone regeneration, resulting in reduced mineral deposition and a lower volume of newly formed bone at the fracture site. Compared with the untreated PSF group, the PSF-VANC and PSF-FK16 groups showed numerically higher BMD, TMD, and BV/TV values. However, none of these between-group differences were statistically significant. Trabecular number (Tb.N) was significantly higher in the PSF group than in the SHAM group ($p < 0.05$) and was also significantly higher in PSF-FK16 than in SHAM ($p < 0.05$). No significant difference in Tb.N was observed between SHAM and PSF-VANC or between the untreated PSF group and either treatment group. Trabecular spacing (Tb.Sp) did not differ significantly among groups. Trabecular thickness (Tb.Th) was significantly lower in the PSF than in the SHAM group ($p < 0.001$). PSF-VANC significantly increased Tb.Th compared with untreated PSF animals ($p < 0.01$). In contrast, Tb.Th did not differ significantly between the PSF-FK16 and PSF groups and remained significantly lower in PSF-FK16 animals than in SHAM animals ($p < 0.01$). Representative micro-CT images and 3D isosurface reconstructions are shown in Figure 5, together with the radiographic osteomyelitis grading score. Radiographic evaluation using Odekerken's osteomyelitis grading scale [20] revealed a significantly higher score in the PSF group than in the SHAM and PSF-FK16 groups ($p < 0.05$). The PSF-VANC group showed a lower osteomyelitis score than the PSF group; however, this difference did not reach statistical significance. These findings indicate that FK-16 significantly reduced the radiographic severity of osteomyelitis compared with unloaded PSF, although it did not significantly improve the quantitative micro-CT parameters of bone healing.

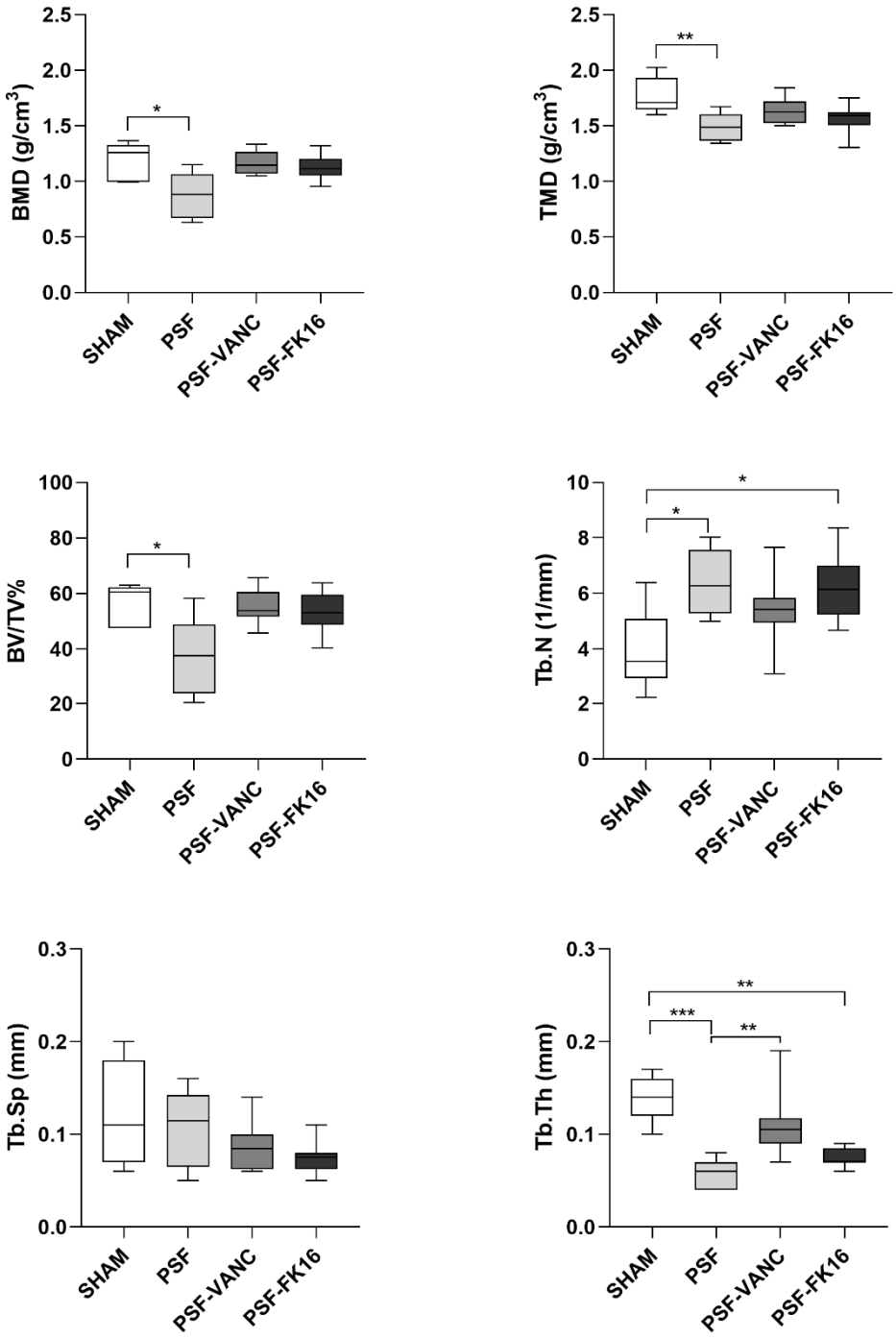


Figure 4. Micro-CT evaluation of bone mineralization and microarchitecture. Bone mineral density (BMD), tissue mineral density (TMD), bone volume fraction (BV/TV), trabecular number (Tb.N), trabecular thickness (Tb.Th), and trabecular spacing (Tb.Sp) were quantified within the predefined volume of interest. Boxes indicate the median and interquartile range, and whiskers indicate the minimum and maximum values (n = 8 per infected group; SHAM, n = 7). Statistical significance is indicated as * $p < 0.05$, ** $p < 0.01$, and *** $p < 0.001$.

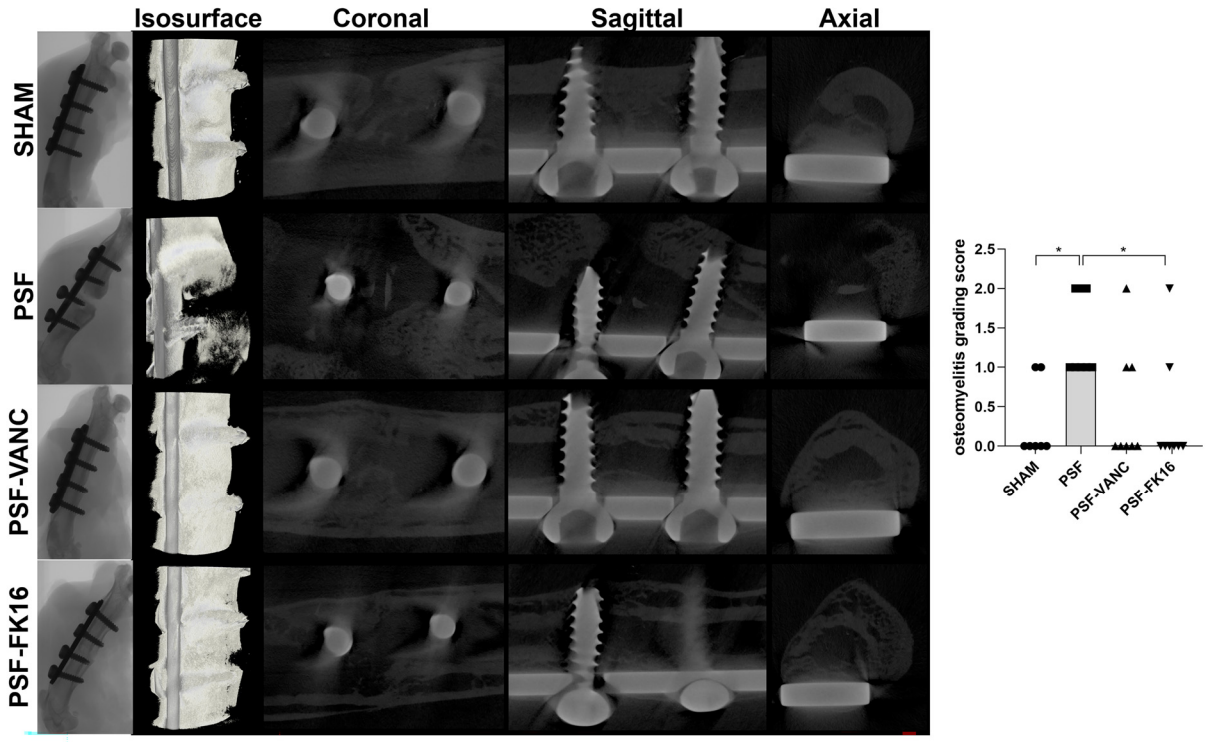


Figure 5. Representative micro-CT images and radiographic osteomyelitis grading. Representative sagittal, coronal, and axial micro-CT images and three-dimensional isosurface reconstructions are shown for each experimental group. Radiographic osteomyelitis severity was assessed using the Odekerken grading scale. Data are presented as individual values with the median (n = 8 per infected group; SHAM, n = 7). Statistical significance is indicated as * $p < 0.05$.

2.2.7. Histological Analysis

Femoral specimens collected on day 56 were evaluated histologically to assess bone healing and inflammation within the defect (Figure 6). Three SHAM specimens (n = 3) and four specimens from each infected group (n = 4) were included in the analysis. One SHAM specimen belonging to the histopathology subset was excluded because postmortem micro-CT examination revealed loss of fixation integrity. In the PSF group, the defect lacked bony bridging and was occupied by abundant, disorganized fibrovascular tissue with multifocal areas of cartilaginous metaplasia. At the level of the fixation plate, inflammatory changes were consistent with a chronic abscess. Both treatment groups had numerically lower histological scores than the untreated PSF group, although the differences were not statistically significant. This trend suggested a reduction in histopathological severity following either vancomycin or FK-16 treatment. In these groups, bony bridging was absent, but cartilaginous tissue predominated over fibrovascular tissue. Inflammatory changes were minimal or nearly absent in both groups.

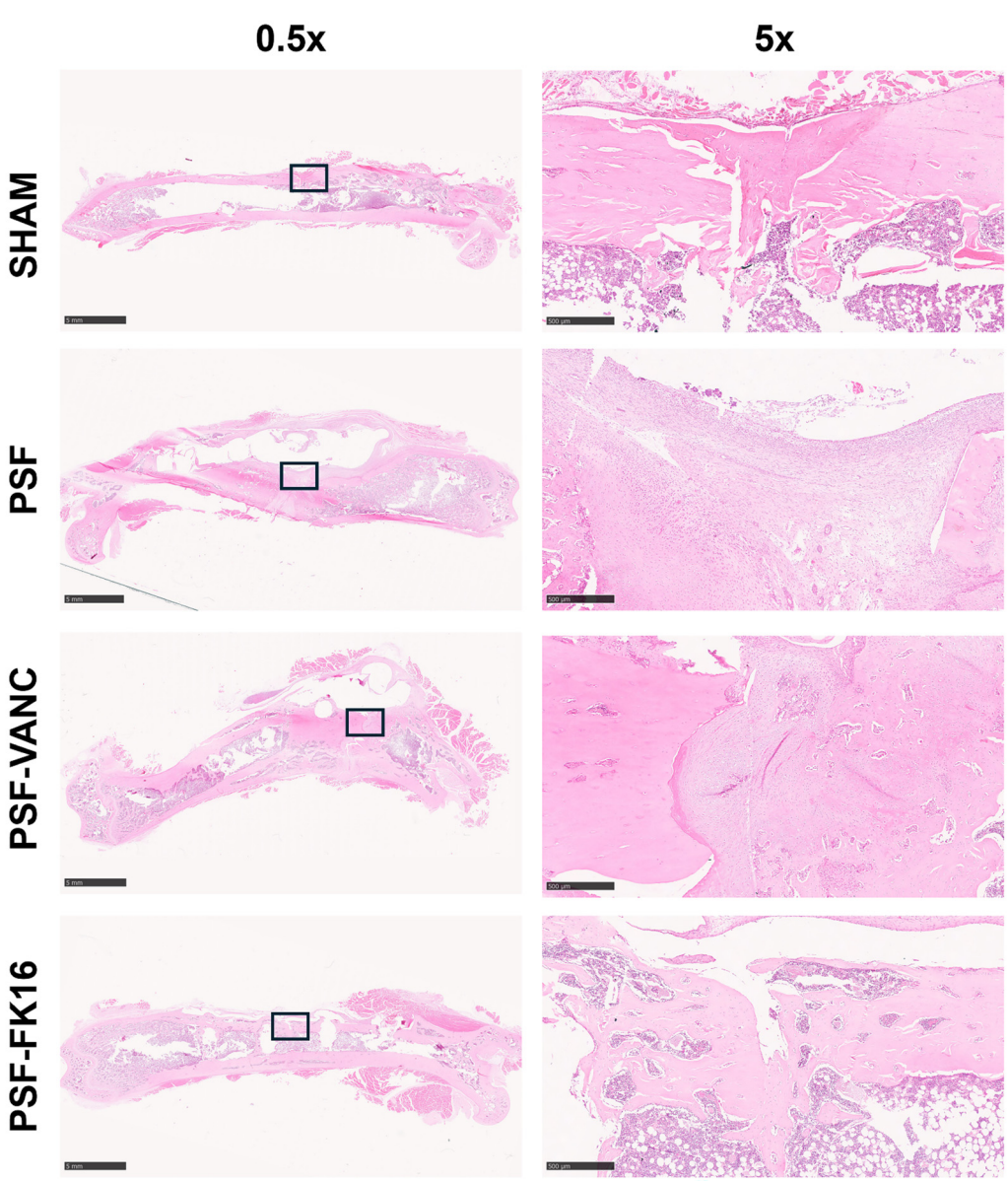


Figure 6. Histological assessment of femoral fracture on day 56. Representative hematoxylin and eosin (H&E)-stained longitudinal sections. Low-magnification overview images are shown in the left column (0.5×; scale bars = 5 mm), while the right column shows higher-magnification views of the regions indicated by the black boxes (5×; scale bars = 500 μm). In the untreated PSF group, bony bridging was absent and the defect was predominantly occupied by abundant, disorganized fibrovascular tissue with multifocal areas of cartilaginous metaplasia; inflammatory changes consistent with a chronic abscess were also observed at the plate level. In both the PSF-VANC and PSF-FK16 groups, bony bridging remained absent, but cartilaginous tissue predominated over fibrovascular tissue and inflammatory changes were minimal or nearly absent compared with untreated PSF.

Gram staining revealed the presence of rare Gram-positive cocci consistent with *Staphylococcus* spp. only in the PSF group (Figure 7).

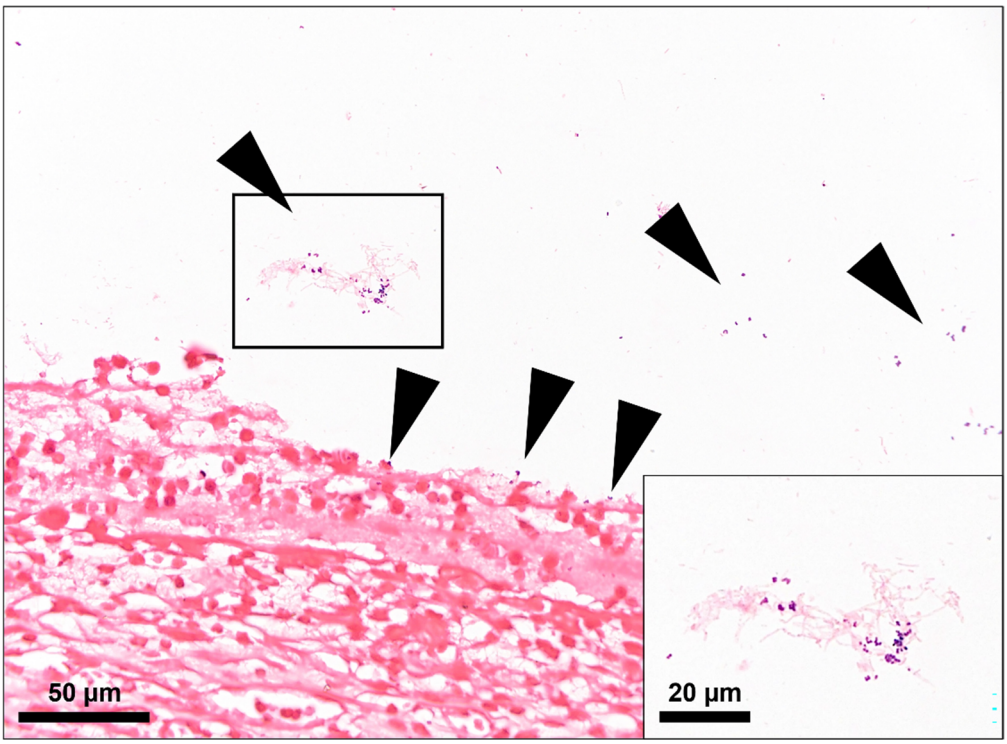


Figure 7. Detection of Gram-positive cocci in the PSF group on day 56. Representative Gram-stained section showing rare purple-staining Gram-positive cocci morphologically consistent with *Staphylococcus* spp. Black arrowheads indicate Gram-positive cocci. The boxed region is shown at higher magnification in the inset. Scale bars: 50 µm (main image) and 20 µm (inset). Gram-positive cocci were detected only in specimens from the untreated PSF group.

The histological score was significantly higher in the untreated PSF group than in the SHAM group ($p < 0.05$), indicating marked histopathological changes in the presence of MRSE infection (Figure 8).

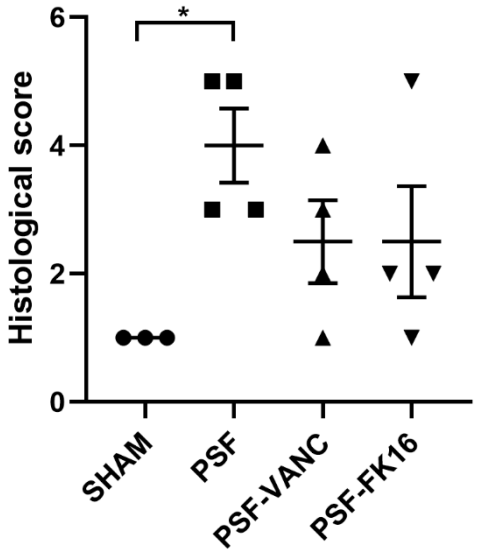


Figure 8. Histological score. Histopathological alterations were assessed using the histological scoring system. Individual histological scores and group mean ± SEM are shown (n = 4 per group, n = 3 SHAM group). Statistical significance is indicated as * $p < 0.05$.

3. Discussion

This study combined two complementary preclinical experiments to address distinct translational questions concerning LL-37-derived antimicrobial peptides: the acute consequences of direct systemic exposure to FK-16 and GF-17, and the local efficacy of FK-16 delivered through peptide-enriched silk fibroin (PSF) in an MRSE-associated femoral nonunion model. Neither peptide caused mortality, persistent neurobehavioral abnormalities, or treatment-related organ lesions after a single intravenous dose. PSF-FK16 demonstrated local antibacterial activity, as culture methods recovered viable MRSE from most untreated infected specimens but from none of the FK-16-treated specimens. However, microbiological control and a lower osteomyelitis score did not translate into significant improvement in quantitative bone-healing parameters at the final time point.

Transient hind-limb paralysis developed 1–3 min after injection in one mouse receiving FK-16 and one treated with GF-17 at 1 mg/kg and resolved spontaneously within 5 min, suggesting an acute adverse effect temporally associated with intravenous administration. Both peptides were administered as a rapid intravenous bolus over approximately 6 s, which may have resulted in transiently elevated systemic peptide concentrations. However, the absence of pharmacokinetic, toxicokinetic, and cardiovascular measurements prevents a definitive interpretation of the underlying mechanism. Although these events were not observed in vehicle-treated or low-dose animals, the limited number of affected mice does not allow the relative contributions of peptide exposure, administration rate, or individual susceptibility to be established. Therefore, the 1 mg/kg dose should not be considered a no-observed-adverse-effect level. The remaining tolerability endpoints did not show a consistent pattern of acute target-organ toxicity. The isolated increase in hemolysis-associated absorbance observed in males treated with low-dose FK-16 lacked a dose–response relationship, was not reproduced in females, and was not accompanied by a time-dependent increase. This finding is relevant because previous in vitro screening identified concentration-dependent hemolytic and mammalian-cell effects for both peptides [14]. More broadly, studies of other synthetic AMPs have shown that in vitro hemolysis and cytotoxicity do not necessarily predict systemic toxicity in vivo, emphasizing the need for peptide-specific in vivo assessment [21]. Similarly, organ weight and histopathological findings did not provide evidence of acute hepatic, renal, or thymic injury. Decreases in ALT activity or total bile acid concentrations are not typical indicators of hepatocellular damage. Serum creatinine concentrations exceeded published reference values for healthy mice in all groups, including controls. These unexpectedly elevated values may reflect assay- or matrix-related analytical bias; however, this explanation could not be confirmed because sample-specific background controls were not performed and residual serum was unavailable for independent reanalysis. The higher creatinine concentration observed in the GF-17 low-dose group lacked a dose–response relationship and was not accompanied by treatment-related renal histopathological alterations. Nevertheless, the possibility of analytical bias also limits confidence in the relative between-group comparison. Accordingly, the assessment of renal tolerability relied primarily on histopathological findings, while recognizing that these findings alone cannot exclude functional renal alterations.

Accordingly, the interpretation of renal tolerability relied primarily on histopathological findings, while recognizing that these findings alone cannot exclude functional renal alterations. Minimal focal hepatic mononuclear infiltrates occurred in control and treated animals, whereas focal tubular basophilia was limited to one mouse, supporting their interpretation as incidental background findings.

The rat experiment reproduced a clinically relevant orthopedic infection. Untreated infected animals generally showed no wound breakdown, purulent discharge, persistent lameness, or weight loss, yet viable MRSE was recovered from three of four specimens,

and micro-CT demonstrated impaired mineralization and osteomyelitis-related changes. This subclinical phenotype is consistent with the original characterization of the model, in which low-grade *S. epidermidis* contamination impaired bone union despite producing few clinical signs [22]. All groups gained weight throughout the follow-up period, indicating the absence of severe systemic deterioration. Nevertheless, the lower percentage weight gain observed in both antimicrobial-treated groups, particularly PSF-FK16, is an unresolved nonspecific finding. Because it was not accompanied by clinical deterioration and was observed with two different antimicrobials, it cannot be attributed directly to either FK-16 toxicity or improved infection control.

Untreated MRSE infection produced a transient systemic inflammatory response on day 7, characterized by increased neutrophils, NLR, and SII. A similar temporal pattern was reported in the previous PSF-based MRSE nonunion study, in which neutrophilia was most evident during the first two postoperative weeks and normalized at later time points [16]. In the present study, vancomycin significantly attenuated all three day-7 indices, whereas FK-16 did not produce statistically significant reductions. This difference should not be interpreted as evidence of inferior local antibacterial efficacy, because (i) the biomarkers are systemic and nonspecific; (ii) the PSF-FK16 formulation releases most of its peptide content within the first 24 h [17]; and (iii) terminal cultures sample a different biological time point. Rather, the findings suggest that FK-16 did not alter the duration of the early systemic response to an extent detectable with the present study design. NLR and SII should therefore remain exploratory in localized orthopedic infection rather than being considered substitutes for local microbiological, imaging, or histopathological assessments.

The absence of detectable MRSE in PSF-FK16 specimens following direct culture and enrichment supports the in vivo antibacterial activity of locally delivered FK-16. This result extends previous in vitro findings against the same clinical isolate, including bactericidal activity within preformed biofilms [14] and the antibacterial activity of FK-16 released from PSF sponges [17]. It is also consistent with earlier proof-of-concept studies in which locally delivered AMPs reduced culture or radiographic evidence of experimental osteomyelitis [23,24]. However, negative culture results should be interpreted as a bacterial burden below the detection limit of the applied methods. Only four specimens per group underwent microbiological analysis; sampling was performed at a single terminal time point, and no molecular, imaging-based, or viability-independent methods were used to investigate residual bacteria or biofilm. Vancomycin was included as an active reference comparator rather than as a dose-matched control. The FK-16 and vancomycin loadings were independently selected on the basis of previous formulation-specific studies and differed in nominal mass, release mechanism, stability, and likely duration of exposure above their respective antibacterial thresholds. The culture-negative findings in both treated groups demonstrate the responsiveness of the model to local antimicrobial therapy.

Untreated infection was associated with lower circulating OPG, later elevation of RANKL, and a persistently reduced OPG/RANKL ratio, indicating a systemic shift toward signaling permissive of osteoclastogenesis. This interpretation is biologically consistent with experimental staphylococcal osteomyelitis. *S. aureus* can induce RANKL expression in osteoblast-lineage cells, and RANKL-dependent osteoclast formation is required for infection-associated bone loss in vivo [18,25]. Although these mechanistic studies have largely focused on *S. aureus*, the direction of change in the present MRSE model supports the broader concept that staphylococcal infection disturbs osteoimmune regulation. Both vancomycin and FK-16 increased circulating OPG concentrations and restored the circulating OPG/RANKL ratio relative to untreated infection, while reductions in RANKL were most evident on day 56. The OPG/RANKL findings must nevertheless be interpreted

cautiously. Circulating concentrations are indirect measurements and do not quantify local availability, osteoclast number, osteoclast activity, or coupling between bone resorption and formation. Moreover, FK-16 improved the systemic ratio without significantly improving BMD, TMD, BV/TV, or trabecular thickness. This discordance indicates that partial normalization of systemic osteoimmunological signaling was insufficient to restore structural healing within 56 days and may reflect either delayed biological recovery or incomplete correspondence between serum markers and the local fracture microenvironment.

The quantitative micro-CT results confirmed that MRSE infection impaired mineral deposition, bone volume, and microarchitecture. FK-16 produced numerical increases in BMD, TMD, and BV/TV compared with unloaded PSF, without reaching statistical significance. Tb.Th also remained below the value observed in the non-infected control group. The higher Tb.N values observed in the PSF and PSF-FK16 groups relative to SHAM should not be interpreted in isolation as improved healing, because these increases occurred alongside thinner trabeculae and reduced mineralization and may therefore represent a more fragmented or immature architecture. Vancomycin significantly improved Tb.Th but did not significantly restore the other quantitative outcomes. In contrast to the quantitative healing parameters, FK-16 significantly reduced the osteomyelitis score. This result is consistent with the culture findings and resembles the radiographic improvement reported after local AMP treatment in a rat osteomyelitis model [24]. The data therefore suggest a partial dissociation between the suppression of infection-related bone destruction and the reconstruction of mechanically and biologically competent bone.

A previous study of vancomycin-nanofunctionalized PSF in the same MRSE model reported more frequent bridging and improved histological outcomes [16], but that formulation used a different loading strategy designed for prolonged antibiotic delivery and therefore cannot be directly compared with the scaffolds used in the present study. By contrast, more than 90% of FK-16 was released from PSF within 24 h in vitro [17]. A rapid initial release may be advantageous for early bacterial killing but may not sustain antimicrobial or immunomodulatory activity throughout the prolonged repair phase. The absence of significant structural recovery may therefore be partly related to the release profile. Early bacterial exposure can initiate tissue necrosis, inflammatory damage, osteoclast activation, biofilm establishment, and disruption of osteoblast function before the bacterial burden is reduced. Subsequent repair may require not only infection control but also prolonged mechanical stability, vascularization, osteogenic signaling, and sufficient time for remodeling. Experimental delivery systems that combine sustained antimicrobial exposure with osteogenic support have achieved concurrent infection suppression and bone formation, including AMP-releasing self-assembling hydrogels and vancomycin/bone morphogenetic protein 2 hydrogels [26,27]. These studies are not directly comparable with the present model, but they support investigating FK-16 formulations with prolonged local retention or combination strategies that separately address bacterial control and regeneration.

Histopathology complemented the microbiological and micro-CT findings by confirming the characteristic MRSE-associated nonunion phenotype in untreated PSF animals. On day 56, PSF specimens showed absent bony bridging, abundant disorganized fibrovascular tissue with cartilaginous metaplasia, and persistent inflammation consistent with chronic abscess formation, resulting in a significantly higher histological score than SHAM. Conversely, both PSF-VANC and PSF-FK16 showed markedly reduced inflammatory changes and more cartilaginous than fibrovascular tissue, although complete bony bridging was still absent. These findings are consistent with the lower osteomyelitis severity observed by micro-CT, particularly in PSF-FK16. This phenotype closely resembles that originally described in the MRSE femoral nonunion model, characterized by

impaired cortical bridging, periosteal reaction, inflammatory tissue, abscess formation, and bone damage [22]. Likewise, Bottagisio et al. [16] reported absent bridging, abundant fibrovascular tissue, chronic abscesses, and necrotic tissue in untreated PSF animals, whereas vancomycin-loaded PSF promoted more advanced bone repair.

Gram staining provided additional, although limited, support for the microbiological findings, as rare Gram-positive cocci morphologically compatible with *Staphylococcus* spp. were observed only in untreated PSF specimens. Their low frequency should not be interpreted as evidence of bacterial absence in the other groups, because Gram staining has inherently low sensitivity [28]. Accordingly, the absence of culture growth in PSF-VANC and PSF-FK16 indicates that no viable MRSE were detected using the methods applied rather than confirmed bacterial eradication, particularly because culture and histology were performed on different specimens. The persistence of incomplete bridging and residual reparative tissue in culture-negative treatment groups further supports a dissociation between microbiological control and complete tissue recovery. A similar distinction emerges from the OPG/RANKL data: both antimicrobial treatments shifted the circulating balance toward a less pro-osteoclastogenic profile, in parallel with reduced local inflammation, but this association should be interpreted cautiously because circulating OPG and RANKL do not directly measure local osteoclast activity. The persistence of impaired structural healing, particularly in PSF-FK16, indicates that normalization of systemic osteoimmunological signaling was not sufficient to restore bone architecture within the study period.

Several limitations temper the conclusions. The mouse study used a single bolus administration, two empirically selected dose levels, no pharmacokinetic or cardiovascular measurements, small sex-specific subgroups, and an observation period of only 24 h; it therefore identifies potential acute risks but cannot establish repeated-dose safety or exposure after scaffold implantation. Importantly, the absence of pharmacokinetic and toxicokinetic measurements prevents the correlation of administered doses with actual systemic exposure and limits the interpretation of potential exposure-dependent adverse effects. Future studies should therefore include dedicated pharmacokinetic and toxicokinetic assessments before progressing toward more comprehensive dose-ranging and repeated-dose safety investigations.

In the rat study, only one MRSE strain was evaluated. Moreover, different specimens were allocated to microbiology and histopathology, preventing direct specimen-level comparisons among culture results, Gram staining, and tissue lesions. The small number of specimens available for each assessment limited the precision of the microbiological estimate and the interpretation of the histopathological findings. In addition, Gram staining has limited sensitivity in orthopedic implant-associated infection [28]. Only rare Gram-positive cocci were identified in the present study, and a contribution from specimen processing cannot be excluded, as plate removal followed by prolonged formalin fixation and ethylenediaminetetraacetic acid (EDTA) decalcification may have reduced the amount of bacterial material retained in the examined sections. Therefore, a negative Gram stain should not be interpreted as evidence of bacterial absence.

Within these limitations, the study provides two relevant translational signals. Direct systemic exposure to FK-16 and GF-17 did not produce detectable acute organ injury; however, the reversible neurological event at 1 mg/kg requires mechanistic clarification and argues against unqualified claims of systemic safety. Locally delivered FK-16 produced evidence of antibacterial activity and reduced osteomyelitis severity, yet did not significantly improve quantitative bone healing by day 56. One SHAM specimen was excluded from micro-CT and histopathological analyses after fixation failure was detected only at terminal postmortem imaging. This endpoint-specific exclusion reduced the SHAM sample size for these analyses and should be considered when interpreting the

corresponding results. Further development should therefore prioritize local pharmacokinetic studies, dose–response assessment, prolonged or tunable release, more sensitive methods for detecting residual bacteria, and strategies that combine antimicrobial delivery with regenerative cues.

This study provides preliminary evidence supporting the potential of LL-37-derived antimicrobial peptides for local treatment of orthopedic implant-associated infections. While single-dose intravenous administration of FK-16 and GF-17 did not produce overt acute organ injury, transient neurological effects at the highest tested dose warrant further investigation. Locally delivered FK-16 demonstrated antibacterial activity against MRSE and reduced radiographic osteomyelitis severity, although significant improvements in quantitative bone healing were not observed by day 56. Further investigations are needed to optimize local peptide delivery, characterize systemic exposure, and evaluate the long-term efficacy and safety of these formulations.

4. Materials and Methods

4.1. Antimicrobial Peptides and Scaffold Preparation

FK-16 (sequence: FKRIVQRIKDFLRNLV) and GF-17 (sequence: GFKRIVQRIKDFLRNLV) are synthetic antimicrobial peptides (AMPs) derived from the human cathelicidin LL-37; both were previously evaluated for antimicrobial activity and mammalian-cell cytocompatibility [14]. They were synthesized and provided in lyophilized form by the University of Pavia (Italy); stock solutions were then prepared in sterile 0.9% NaCl immediately before intravenous administration.

Osteoinductive peptide-enriched silk fibroin sponges (PSF) were prepared by KLISBio srl (Bresso, Milan, Italy) following previously published procedures [16,17]. Briefly, silk fibroin was extracted from degummed *Bombyx mori* cocoons, dissolved in lithium bromide, and dialyzed to obtain an aqueous fibroin solution. An osteoinductive fraction of fibroin-derived anionic peptides was obtained through enzymatic digestion with α-chymotrypsin and subsequently incorporated into the fibroin solution. The resulting mixture was lyophilized to produce porous PSF sponges used as delivery matrices for FK-16 or vancomycin.

The FK-16 loading was selected based on previous in vitro experiments evaluating peptide loading, release, antimicrobial activity against the MRSE strain, and mammalian-cell compatibility [17]. These experiments demonstrated rapid FK-16 release from PSF scaffolds and bactericidal activity against MRSE, supporting the selection of this formulation for subsequent in vivo evaluation. Vancomycin was included as an active comparator based on previous experience with PSF-mediated local antibiotic delivery in the same rat model of MRSE-associated femoral nonunion [16]. The FK-16 and vancomycin loadings were selected separately for the two formulations and were not intended to provide dose-equivalent antimicrobial exposure. Accordingly, the study was designed to assess the antibacterial efficacy of each treatment relative to unloaded PSF, rather than to establish a dose-equivalent comparison between FK-16 and vancomycin.

Considering an average dry scaffold weight of 2.8 mg, the nominal FK-16 loading of 307 μg per mg of dry scaffold corresponded to approximately 860 μg of FK-16 per scaffold. Each scaffold was loaded with 10 μL of peptide solution at a nominal concentration of approximately 86.0 mg/mL. The reported amount of approximately 860 μg per scaffold was calculated from the initial formulation and was not independently quantified in the scaffolds used for the in vivo experiments. This loading corresponded to a peptide-to-dry-scaffold mass ratio of 30.7% *w*/*w*. This nominal loading was selected based on our previous in vitro time–kill assays, in which FK-16-loaded PSF scaffolds demonstrated strong antibacterial activity against the same MRSE strain [17].

Similarly, the nominal vancomycin (Merck) loading of 51.8 μg per mg of dry scaffold corresponded to approximately 145 μg per scaffold and required a loading-solution concentration of approximately 14.5 mg/mL. This loading corresponded to a vancomycin-to-dry-scaffold mass ratio of 5.18% *w*/*w*. The scaffolds were then air-dried overnight under aseptic conditions with ultraviolet exposure and stored at −20 °C until use. Unloaded PSF scaffolds were used as controls.

4.2. Ethics

All animal procedures were approved by the competent institutional animal-welfare bodies of Fondazione Istituto Insubrico Ricerca per la Vita (Permit No. 188/2025-PR) and the Mario Negri Institute for Pharmacological Research (Permit No. 726/2025-PR) for mouse and rat studies, respectively. Experiments were conducted in accordance with Directive 2010/63/EU and Italian Legislative Decree 26/2014. Anesthesia, analgesia, humane endpoints, and postoperative monitoring were applied to minimize animal pain and distress.

4.3. Animals and Experimental Design

The acute tolerability study included 36 six-week-old BALB/c mice (18 males and 18 females; Envigo-Inotiv, Italy). Both sexes were included to account for potential sex-related differences in acute systemic responses to the peptides and to provide a more comprehensive preliminary tolerability assessment. Given the limited sample size of the sex-specific subgroups, the evaluation of potential sex-related effects was considered exploratory.

Mice were allocated to five groups: vehicle control (n = 6; 3 males, 3 females), FK-16 at 0.1 mg/kg (low dose) (n = 6; 3 males, 3 females), FK-16 at 1 mg/kg (high dose) (n = 9; 5 males, 4 females), GF-17 at 0.1 mg/kg (n = 6; 3 males, 3 females), and GF-17 at 1 mg/kg (n = 9; 4 males, 5 females). Upon arrival, mice were acclimatized for 7 days and housed up to five animals per cage under a 12-h light/dark cycle with ad libitum access to food and water. Environmental enrichment consisted of shelters. In the absence of pharmacokinetic or toxicokinetic data, the intravenous experiment was designed as a preliminary in vivo assessment aimed at identifying potential acute adverse effects following direct systemic exposure, rather than establishing a comprehensive safety or pharmacokinetic profile. This approach was supported by our previous in vitro findings demonstrating concentration-dependent hemolytic activity and mammalian-cell toxicity of both peptides [14], which highlighted the need for further evaluation of their systemic tolerability. Accordingly, doses of 0.1 and 1 mg/kg were empirically selected as exploratory challenge levels, with a tenfold separation intended to facilitate the identification of potential dose-related adverse effects. These doses were not intended to represent therapeutic or established safe exposure levels. Furthermore, intravenous administration was not intended to reproduce the pharmacokinetic profile associated with local scaffold implantation. Allocation was stratified by sex. Within each sex, animals were manually selected from the cage without a predetermined order and assigned to the treatment groups. The larger high-dose groups were prespecified to increase the amount of tolerability information obtained at the maximum tested dose.

The efficacy study included 32 twelve-week-old male Wistar rats (340.6 ± 12.2 g; Envigo-Inotiv), allocated to four groups (n = 8 each): non-infected control (SHAM), infected control receiving unloaded PSF (PSF), infected group receiving vancomycin-loaded PSF (PSF-VANC), and infected group receiving FK-16-loaded PSF (PSF-FK16). Rats were housed two per cage, acclimatized for 7 days, and maintained under a 12-h light/dark cycle with ad libitum access to food and water. Environmental enrichment consisted of shelters and wooden blocks. Rats were manually selected from the cage in no

predetermined order and assigned to the treatment groups by an investigator not involved in treatment administration. Allocation was balanced according to baseline body weight.

Investigators performing clinical observations and FOB assessments in mice were not blinded to treatment allocation. Samples were identified using coded labels, and investigators conducting biochemical assays, microbiological analyses, micro-CT measurements, histopathological scoring, and statistical analyses were blinded to treatment allocation. No formal a priori exclusion criterion specifically addressing fixation failure was defined. After terminal imaging, endpoint-specific evaluability was assessed. When postmortem micro-CT demonstrated loss of fixation integrity, the affected specimens were considered unsuitable for micro-CT and histopathological assessment because mechanical instability invalidates the standardized osteotomy model. Data collected longitudinally before euthanasia remained eligible for analysis.

4.4. Single-Dose Intravenous Tolerability Study in Mice

This study evaluated the acute intravenous tolerability of FK-16 and GF-17 over 24 h. Immediately before administration, FK-16 and GF-17 were dissolved in sterile 0.9% NaCl to final concentrations of 0.01 and 0.10 mg/mL for the 0.1 and 1 mg/kg dose groups, respectively. Vehicle-control animals received sterile 0.9% NaCl alone. Each formulation was administered into a lateral tail vein using a sterile 29-gauge needle at a dose volume of 10 mL/kg, calculated individually from the body weight recorded immediately before dosing. Each solution was administered intravenously over approximately 6 s. Animals were continuously observed during administration and for the first 15 min thereafter. Functional and clinical assessments were subsequently performed at 15 and 30 min, and at 1, 2, 3, 4, 6, and 24 h. The FOB assessed posture, gait, motor activity, muscle tone, sensory responses, respiration, autonomic signs, and abnormal behavior. Mortality and the onset, duration, and reversibility of any clinical sign were recorded. Body weight was recorded before injection and after 24 h.

4.4.1. Blood Collection and Hemolysis Assay

At 3 h after administration, blood was collected into K_2-EDTA-treated microtubes (BD Microtainer MAP, catalog no. 363706; Becton, Dickinson and Company, Franklin Lakes, NJ, USA) for the assessment of hemolysis-associated plasma absorbance. At 24 h, mice were weighed, anesthetized with 4% isoflurane (Merial, Italy), and terminal blood samples collected by cardiac puncture were immediately divided between K_2-EDTA-treated microtubes and serum collection tubes without anticoagulant. EDTA-anticoagulated blood was centrifuged at 1500× *g* for 15 min at 4 °C, and the resulting plasma was used to measure absorbance at 540 nm. Because no calibration against known free-hemoglobin concentrations was performed, results were expressed as absorbance units rather than as absolute plasma hemoglobin concentrations. Blood collected in serum tubes was allowed to clot undisturbed for 30 min at room temperature (RT) and was then centrifuged at 1500× *g* for 15 min at 4 °C. The resulting serum was used to measure ALT, AST, creatinine, and total bile acids. Plasma and serum aliquots were stored at −80 °C until analysis and were not subjected to repeated freeze–thaw cycles.

4.4.2. Clinical Chemistry

Serum creatinine was measured as an exploratory biochemical parameter using a commercially available enzymatic colorimetric assay (Creatinine Assay Kit, catalog no. MAK475; Sigma-Aldrich, USA). Prior to analysis, serum samples were deproteinized using 10 kDa molecular-weight-cutoff spin filters, according to the manufacturer's recommendations. Absorbance values were corrected by subtracting the reagent blank, as

specified in the assay protocol. No sample-specific background controls were performed. Hepatic biochemical markers were assessed through the determination of ALT, AST, and total bile acids using commercial assay kits (RayBiotech, USA; Sigma-Aldrich, USA; and Abbexa, UK, respectively). Samples were analyzed in duplicate, and concentrations or enzyme activities were calculated according to the manufacturers' calibration procedures.

4.4.3. Necropsy and Histopathology

After terminal blood collection, mice were euthanized by cervical dislocation under anesthesia. The liver, kidneys, spleen, and thymus were examined macroscopically and weighed. Relative organ weights were calculated as organ weight divided by terminal body weight × 100. Tissues were fixed in 10% neutral-buffered formalin, paraffin-embedded, sectioned at 3 μm, and stained with hematoxylin and eosin. Slides were evaluated by a board-certified veterinary pathologist blinded to treatment allocation (Inotiv, Italy).

4.5. In Vivo Antimicrobial Efficacy in A Rat Model of Orthopedic Infection

4.5.1. Bacterial Strain and Characterization

The methicillin-resistant *Staphylococcus epidermidis* (MRSE) clinical strain GOI1153754-03-14 was isolated from an infected knee prosthesis of a patient undergoing revision surgery at the IRCCS Galeazzi Orthopedic Institute (Milan, Italy), as previously described by Lovati et al. [22]. Previous antimicrobial susceptibility testing demonstrated resistance to benzylpenicillin, oxacillin, cefazolin, rifampicin, and levofloxacin, while susceptibility to vancomycin was retained [22]. The strain was previously characterized as a strong biofilm producer in vitro and demonstrated the ability to induce implant-associated osteomyelitis and femoral nonunion in a rat model [22]. These characteristics supported its selection for the present study.

4.5.2. Surgical Approach

Surgery was performed under aseptic conditions using a previously described model [16,22]. Briefly, a 1-mm mid-diaphyseal osteotomy was created in the right femur and stabilized using a stainless-steel plate and bicortical screws (all from Zimmer, Germany). The MRSE strain GOI1153754-03-14 was cultured, and the inoculum was adjusted to 3×10^5 CFU in 30 μL. The bacterial concentration was confirmed by quantitative culture. After fixation, infected animals received the bacterial suspension directly into the osteotomy, whereas non-infected controls received 30 μL of sterile vehicle and the unloaded scaffold (SHAM). The defect was then filled with PSF, PSF-VANC, or PSF-FK16. Soft tissues were closed in layers. Animals received perioperative analgesia and supportive care in accordance with institutional veterinary protocols, as reported elsewhere [16,22]. Animals were examined daily for wound condition, mobility, weight-bearing, clinical signs of infection, and distress. Body weight was recorded weekly. On day 56, animals were anesthetized for terminal blood collection and euthanized by CO_2 exposure. All femurs were scanned by micro-CT; only evaluable datasets were included in the quantitative imaging analysis. Subsequently, specimens were randomly assigned to microbiological analysis or histopathology.

4.5.3. Blood Collection and Systemic Biomarkers

Blood was collected from the tail vein on days 0, 2, 7, and 28 and by cardiac puncture on day 56. Approximately 150 μL was collected into K_2-EDTA tubes for hematology, and 200 μL was collected into serum tubes. Serum was allowed to clot for 30 min, centrifuged at 2000× *g* for 10 min, aliquoted, and stored at −80 °C.

Absolute neutrophil, lymphocyte, and platelet counts were measured using a Sysmex XT-1800 analyzer (Dasit, Italy). The NLR was calculated as neutrophils/lymphocytes [29], and the SII as platelets × neutrophils/lymphocytes [30].

To investigate the interaction between systemic inflammation and bone remodeling, circulating OPG and RANKL were quantified in serum samples using methods similar to those previously described in studies of osteoarticular infections [19]. Briefly, serum OPG and soluble RANKL concentrations were measured using commercially available rat-specific immunoassays according to the manufacturers' instructions (Neobiotech, 92000 Nanterre, France). Samples, standards, and quality controls were analyzed using the recommended assay conditions. Optical density was measured with a microplate reader at 450 nm, and analyte concentrations were calculated from the corresponding standard curves. OPG and RANKL concentrations were expressed as pg/mL. The OPG/RANKL ratio was calculated for each animal by dividing the serum OPG concentration by the corresponding RANKL concentration measured at the same time point. This ratio was used as an indirect indicator of the systemic balance between anti-resorptive and pro-osteoclastogenic signaling. Higher values were interpreted as reflecting a relative predominance of OPG-mediated inhibition of osteoclastogenesis, whereas lower values indicated a shift toward RANKL-mediated osteoclastogenic activity.

4.5.4. Micro-CT Imaging

Femurs were analyzed using a SkyScan 1276 micro-CT scanner (Bruker, Belgium). Scans were acquired with an isotropic voxel size of 9 μm, an X-ray tube voltage of 100 kV, a current of 90 μA, a 1-mm aluminum filter, an exposure time of 500 ms, frame averaging of 3, and a rotation step of 0.5° over a full 360° rotation.

The acquired datasets were reconstructed into three-dimensional images using NRecon software (v. 2.3.1.1, Bruker). To ensure consistency among samples, identical reconstruction parameters were applied to all datasets: Ring Artifact Correction = 4, Beam Hardening Correction = 65%, and Gaussian Smoothing = 2. Reconstruction was performed using a grayscale range of 0.00–0.40. These settings were selected to optimize bone visualization while minimizing artifacts generated by the osteosynthesis hardware.

All reconstructed datasets were subsequently reoriented using DataViewer software (v. 1.7.0.1, Bruker). A volume of interest (VOI) measuring 500 × 400 × 300 pixels was defined and extracted for each specimen, centered within the region between the two fixation screws. The resulting volumes were used for subsequent quantitative analyses.

Bone healing-related morphometric parameters were quantified using CTAn software (v. 1.25.0.0, Bruker), including BV/TV. A single global threshold, defined as the mean of the individual thresholds obtained using the 3D Otsu automatic thresholding method, was applied to all samples before morphometric measurements were performed [16].

In addition, a calibrated version of CTAn software was used to measure BMD, TMD, Tb.N, Tb.Th, and Tb.Sp. Mineral density calibration was performed using two density phantoms (0.25 and 0.75 g/cm^3; Bruker) scanned and reconstructed under the same acquisition and reconstruction conditions as the experimental specimens. Radiographic signs of osteomyelitis were assessed on the reconstructed images by a blinded observer using the Odekerken scale [20].

4.5.5. Microbiological Evaluation

Each sample assigned to microbiological analysis comprised the femur, plate, and screws. Under aseptic conditions, each sample was immersed in 10 mL of sterile saline containing 0.1% *w*/*v* dithiothreitol. Samples were transported at 4 °C and processed within 5 h. After sonication for 5 min at 45 kHz in an ultrasonic bath at RT and subsequent vortexing, the suspension was centrifuged at 2486× *g* for 15 min at RT. The resulting pellets

were resuspended in 1 mL of sterile saline. An aliquot of 100 µL from each of six serial dilutions was plated in triplicate on tryptic soy agar (TSA) and mannitol salt agar (MSA) and incubated at 37 °C for 24 h. Direct counts were reported as average CFU/mL per experimental group, with a limit of detection (LOD) of 10 CFU/mL. For enrichment, 100 µL of the resuspended pellet was inoculated into 10 mL of brain heart infusion broth (BHI) and incubated at 37 °C for up to 14 days, with aliquots of 100 µL plated on TSA at 48-h intervals or whenever turbidity developed. Recovered isolates were identified using the VITEK 2 Compact system with VITEK 2 GP identification and AST 632 susceptibility-testing cards (bioMérieux, Craponne, France) and compared with the inoculated MRSE strain.

4.5.6. Histological and Histopathological Analysis

Femurs assigned to histology were fixed in 10% neutral-buffered formalin for 5 days, decalcified using 10% EDTA (pH 8) for 30 days, paraffin-embedded, and sectioned at 5 µm. Sections were stained with hematoxylin and eosin (H&E) or subjected to Gram staining to detect residual bacteria. Bone healing and inflammation were evaluated using a rat-specific histopathological score ranging from 0 to 5 (Appendix A, Table A1), as previously described [16]. A board-certified veterinary pathologist evaluated all slides blinded to treatment allocation.

4.6. Statistical Analysis

Sample sizes were selected using Mead's Resource Equation, taking into account the number of treatment groups, the experimental design, and the sampling scheme. Because this approach was not based on an expected effect size for a prospectively specified primary outcome, no single outcome was used for a formal power calculation. Both the acute tolerability study and the rat efficacy study were therefore considered exploratory. The individual animal was considered the experimental unit, and technical replicates were averaged before statistical analysis. Analyses were conducted on an endpoint-specific basis using all evaluable animals. Accordingly, the SHAM animal with fixation failure remained included in longitudinal clinical, body-weight, and blood-based analyses but was excluded from micro-CT and histopathological analyses. Normality was assessed using the Shapiro–Wilk test. When the assumptions required for parametric analysis were not adequately met, nonparametric methods were used.

Mouse body-weight changes were analyzed by ordinary two-way ANOVA, with treatment and sex as between-subject factors. When appropriate, Dunnett's multiple-comparisons test was used to compare each treatment group with the vehicle group separately within each sex. Because several animals showed no change in body weight, separate Kruskal–Wallis tests were also performed for females and males.

Hemolysis assay absorbance values measured at 540 nm were analyzed by three-way repeated-measures ANOVA, with treatment and sex as between-subject factors and time as the within-subject factor, followed by Dunnett's multiple-comparisons test.

Biochemical parameters (ALT, AST, creatinine, and bile acids) and organ weights were analyzed by ordinary two-way ANOVA, with treatment and sex as between-subject factors. When appropriate, treatment groups were compared with the vehicle group separately within each sex using Dunnett's test.

Rat body-weight data were analyzed by two-way repeated-measures ANOVA, with treatment as the between-subject factor and time as the within-subject factor. Sphericity was not assumed, and the Greenhouse–Geisser correction was applied to effects involving time. Significant treatment-by-time interactions were followed by Tukey-adjusted comparisons at each time point.

Neutrophil counts, NLR, and SII were analyzed using mixed-effects models including treatment, time, and their interaction. Pairwise comparisons at individual time points

were adjusted using Tukey's test. OPG, RANKL, and the OPG/RANKL ratio were analyzed by two-way repeated-measures ANOVA followed by Tukey's test. Micro-CT outcomes and radiographic osteomyelitis scores were analyzed using the Kruskal–Wallis test, followed, when appropriate, by Dunn's multiple-comparisons test.

Continuous parametric data are presented as mean ± standard error of the mean (SEM), whereas continuous nonparametric data are reported as medians. Ordinal and histopathological data are summarized as the number of affected animals over the total number examined (n/N), together with the corresponding severity grade. Values of $p < 0.05$ were considered statistically significant. All statistical analyses were performed using GraphPad Prism version 8 (GraphPad Software, San Diego, CA, USA).

Author Contributions: Conceptualization, V.P. and A.B.L.; methodology, V.P., S.M., G.M., M.A., B.C., C.R., D.S., F.S., E.D.V., E.G., and A.B.L.; validation, V.P., C.R., E.G., and A.B.L.; formal analysis, V.P., S.M., G.M., M.A., B.C., C.R., D.S., F.S., E.G., and A.B.L.; investigation, V.P., S.M., G.M., M.A., B.C., C.R., D.S., F.S., E.D.V., E.G., and A.B.L.; resources, A.B.L., C.R., F.S., and E.G.; data curation, V.P., M.A., C.R., F.S., E.D.V., E.G., and A.B.L.; writing—original draft preparation, V.P., M.A., C.R., F.S., E.G., and A.B.L.; writing—review and editing, V.P., M.A., C.R., F.S., E.G., and A.B.L.; visualization, A.B.L. and V.P.; supervision, A.B.L.; project administration, A.B.L.; funding acquisition, A.B.L. All authors have read and agreed to the published version of the manuscript.

Funding: This work was supported by the Italian Ministry of Health, "Ricerca Corrente". The funder had no role in the design of the study; in the collection, analysis, or interpretation of the data; in the writing of the manuscript; or in the decision to submit the manuscript for publication.

Institutional Review Board Statement: The animal study protocol was approved by the Institutional Ethics Committee of Fondazione Istituto Insubrico Ricerca per la Vita (Permit No. 188/2025-PR, approved on 14 March 2025) and the Mario Negri Institute for Pharmacological Research (Permit No. 726/2025-PR, approved on 30 September 2025) for mouse and rat studies, respectively. Experiments were conducted in accordance with Directive 2010/63/EU and Italian Legislative Decree 26/2014.

Data Availability Statement: The original data presented in the study are openly available in the Zenodo repository at the following DOI: 10.5281/zenodo.22828345 (https://zenodo.org/records/22828345).

Acknowledgments: ChatGPT (OpenAI; version 5.6) was used to assist with language editing, readability improvement, and the preparation of the graphical abstract. The authors reviewed and approved all AI-assisted content and take full responsibility for the final manuscript.

Conflicts of Interest: The authors declare no conflicts of interest.

Abbreviations

The following abbreviations are used in this manuscript:

AMP/AMPs	Antimicrobial peptide(s)
ALT	Alanine aminotransferase
ANOVA	Analysis of variance
AST	Aspartate aminotransferase
BHI	Brain heart infusion broth
BMD	Bone mineral density
BMP-2	Bone morphogenetic protein 2
BV/TV	Bone volume fraction
CFU	Colony-forming units
EDTA	Ethylenediaminetetraacetic acid
FOB	Functional Observational Battery

FRI	Fracture-related infection
H&E	Hematoxylin and eosin
LOD	Limit of detection
micro-CT	Micro-computed tomography
MRSE	Methicillin-resistant *Staphylococcus epidermidis*
MSA	Mannitol salt agar
NLR	Neutrophil-to-lymphocyte ratio
OPG	Osteoprotegerin
PSF	Peptide-enriched silk fibroin
PSF-FK16	FK-16-loaded PSF scaffold group
PSF-VANC	Vancomycin-loaded PSF scaffold group
RANKL	Receptor activator of nuclear factor-κB ligand
RT	Room temperature
SEM	Standard error of the mean
SF	Silk fibroin
SHAM	Non-infected control group
SII	Systemic immune-inflammation index
Tb.N	Trabecular number
Tb.Sp	Trabecular spacing
Tb.Th	Trabecular thickness
TMD	Tissue mineral density
TSA	Tryptic soy agar
UV	Ultraviolet
VOI	Volume of interest

Appendix A

Table A1. Histopathological scoring system reported by Bottagisio et al. [16].

0 = normal bone
1 = complete bony bridging without inflammation, absence to slight periosteal reaction, no to slight fibrovascular tissue
2 = complete bony bridging, minimal to slight inflammation, minimal to slight periosteal reaction and minimal to slight fibrovascular tissue
3 = absence of bony bridging, minimal to slight inflammation, slight to moderate fibrovascular tissue with or without cartilaginous metaplasia
4 = absence of bony bridging, slight to moderate inflammation, moderate to marked fibrovascular tissue with or without cartilaginous metaplasia
5 = absence of bony bridging, marked to severe inflammation, marked to severe fibrovascular tissue with or without cartilaginous metaplasia

References

1. Harris, L.G.; Richards, R.G. Staphylococci and implant surfaces: A review. *Injury* **2006**, *37*, S3–S14.
2. Metsemakers, W.J.; Morgenstern, M.; McNally, M.A.; Moriarty, T.F.; McFadyen, I.; Scarborough, M.; Athanasou, N.A.; Ochsner, P.E.; Kuehl, R.; Raschke, M.; et al. Fracture-related infection: A consensus on definition from an international expert group. *Injury* **2018**, *49*, 505–510.
3. Metsemakers, W.J.; Morgenstern, M.; Senneville, E.; Borens, O.; Govaert, G.A.M.; Onsea, J.; Depypere, M.; Richards, R.G.; Trampuz, A.; Verhofstad, M.H.J.; et al. General treatment principles for fracture-related infection: Recommendations from an international expert group. *Arch. Orthop. Trauma Surg.* **2020**, *140*, 1013–1027.
4. Depypere, M.; Sliepen, J.; Onsea, J.; Debaveye, Y.; Govaert, G.A.M.; IJpma, F.F.A.; Zimmerli, W.; Metsemakers, W.J. The microbiological etiology of fracture-related infection. *Front. Cell. Infect. Microbiol.* **2022**, *12*, 934485.
5. Van Agtmaal, J.L.; Verheul, M.; Vonken, L.; Helsen, K.; Vargas Guerrero, M.G.; Van Hoogstraten, S.W.G.; Hurck, B.J.; Pilla, G.; Trinh, I.; De Bruijn, G.J.; et al. Antimicrobial resistance in orthopedics: Microbial insights, clinical impact, and the necessity of a multidisciplinary approach. A review. *Acta Orthop.* **2025**, *96*, 555–568.

6. Liu, Y.; Li, X.; Liang, A. Current research progress of local drug delivery systems based on biodegradable polymers in treating chronic osteomyelitis. *Front. Bioeng. Biotechnol*. **2022**, *10*, 1042128.
7. Alzain, M.; Daghistani, H.; Shamrani, T.; Almoghrabi, Y.; Daghistani, Y.; Alharbi, O.S.; Sait, A.M.; Mufrrih, M.; Alhazmi, W.; Alqarni, M.A.; et al. Antimicrobial peptides: Mechanisms, applications, and therapeutic potential. *Infect. Drug Resist.* **2025**, *18*, 4385–4426.
8. Andersson, D.I.; Hughes, D.; Kubicek-Sutherland, J.Z. Mechanisms and consequences of bacterial resistance to antimicrobial peptides. *Drug Resist. Updat*. **2016**, *26*, 43–57.
9. Mookherjee, N.; Anderson, M.A.; Haagsman, H.P.; Davidson, D.J. Antimicrobial host defence peptides: Functions and clinical potential. *Nat. Rev. Drug Discov.* **2020**, *19*, 311–332.
10. Voronko, O.E.; Khotina, V.A.; Kashirskikh, D.A.; Lee, A.A.; Gasanov, V.A. Antimicrobial peptides of the cathelicidin family: Focus on LL-37 and its modifications. *Int. J. Mol. Sci.* **2025**, *26*, 8103.
11. Wang, G.; Epand, R.F.; Mishra, B.; Lushnikova, T.; Thomas, V.C.; Bayles, K.W.; Epand, R.M. Decoding the functional roles of cationic side chains of the major antimicrobial region of human cathelicidin LL-37. *Antimicrob. Agents Chemother.* **2012**, *56*, 845–856.
12. Mishra, B.; Golla, R.M.; Lau, K.; Lushnikova, T.; Wang, G. Anti-staphylococcal biofilm effects of human cathelicidin peptides. *ACS Med. Chem. Lett.* **2015**, *7*, 117–121.
13. Mishra, B.; Wang, G. Titanium surfaces immobilized with the major antimicrobial fragment FK-16 of human cathelicidin LL-37 are potent against multiple antibiotic-resistant bacteria. *Biofouling* **2017**, *33*, 544–555.
14. Pennone, V.; Angelini, E.; Sarlah, D.; Lovati, A.B. Antimicrobial properties and cytotoxicity of LL-37-derived synthetic peptides to treat orthopedic infections. *Antibiotics* **2024**, *13*, 764.
15. Melke, J.; Midha, S.; Ghosh, S.; Ito, K.; Hofmann, S. Silk fibroin as biomaterial for bone tissue engineering. *Acta Biomater.* **2016**, *31*, 1–16.
16. Bottagisio, M.; Palombella, S.; Lopa, S.; Sangalli, F.; Savadori, P.; Biagiotti, M.; Sideratou, Z.; Tsiourvas, D.; Lovati, A.B. Vancomycin-nanofunctionalized peptide-enriched silk fibroin to prevent methicillin-resistant Staphylococcus epidermidis-induced femoral nonunions in rats. *Front. Cell. Infect. Microbiol.* **2023**, *12*, 1056912.
17. Pennone, V.; Meogrossi, G.; Carenzi, G.; Sarlah, D.; Biagiotti, M.; Lovati, A.B. Development of silk fibroin-based sponges loaded with LL-37-derived peptides for the control of orthopedic infections. *Int. J. Mol. Sci.* **2025**, *26*, 7775.
18. Campbell, M.J.; Bustamante-Gomez, C.; Fu, Q.; Beenken, K.E.; Reyes-Pardo, H.; Smeltzer, M.S.; O'Brien, C.A. RANKL-mediated osteoclast formation is required for bone loss in a murine model of Staphylococcus aureus osteomyelitis. *Bone* **2024**, *187*, 117181.
19. Galliera, E.; Massaccesi, L.; Suardi, V.; de Vecchi, E.; Villa, F.; Yi, Z.; Suo, G.; Lovati, A.B.; Logoluso, N.; Corsi Romanelli, M.M.; et al. sCD14-ST and related osteoimmunological biomarkers: A new diagnostic approach to osteomyelitis. *Diagnostics* **2024**, *14*, 1588.
20. Odekerken, J.C.; Arts, J.J.; Surtel, D.A.; Walenkamp, G.H.; Welting, T.J. A rabbit osteomyelitis model for the longitudinal assessment of early post-operative implant infections. *J. Orthop. Surg. Res.* **2013**, *8*, 38.
21. Greco, I.; Molchanova, N.; Holmedal, E.; Jenssen, H.; Hummel, B.D.; Watts, J.L.; Håkansson, J.; Hansen, P.R.; Svenson, J. Correlation between hemolytic activity, cytotoxicity and systemic in vivo toxicity of synthetic antimicrobial peptides. *Sci. Rep.* **2020**, *10*, 13206.
22. Lovati, A.B.; Romanò, C.L.; Bottagisio, M.; Monti, L.; De Vecchi, E.; Previdi, S.; Accetta, R.; Drago, L. Modeling Staphylococcus epidermidis-induced non-unions: Subclinical and clinical evidence in rats. *PLoS ONE* **2016**, *11*, e0147447.
23. Faber, C.; Stallmann, H.P.; Lyaruu, D.M.; Joosten, U.; von Eiff, C.; van Nieuw Amerongen, A.; Wuisman, P.I.J.M. Comparable efficacies of the antimicrobial peptide human lactoferrin 1-11 and gentamicin in a chronic methicillin-resistant Staphylococcus aureus osteomyelitis model. *Antimicrob. Agents Chemother.* **2005**, *49*, 2438-2444.
24. Melicherčík, P.; Čeřovský, V.; Nešuta, O.; Jahoda, D.; Landor, I.; Ballay, R.; Fulín, P. Testing the efficacy of antimicrobial peptides in the topical treatment of induced osteomyelitis in rats. *Folia Microbiol.* **2018**, *63*, 97-104.
25. Somayaji, S.N.; Ritchie, S.; Sahraei, M.; Marriott, I.; Hudson, M.C. Staphylococcus aureus induces expression of receptor activator of NF-kappaB ligand and prostaglandin E2 in infected murine osteoblasts. *Infect. Immun.* **2008**, *76*, 5120-5126.
26. Jung, S.W.; Oh, S.H.; Lee, I.S.; Byun, J.H.; Lee, J.H. In situ gelling hydrogel with antibacterial activity and bone healing property for treatment of osteomyelitis. *Tissue Eng. Regen. Med.* **2019**, *16*, 479-490.
27. Yang, G.; Huang, T.; Wang, Y.; Wang, H.; Li, Y.; Yu, K.; Dong, L. Sustained release of antimicrobial peptide from self-assembling hydrogel enhanced osteogenesis. *J. Biomater. Sci. Polym. Ed.* **2018**, *29*, 1812-1824.

28. Ouyang, Z.; Zhai, Z.; Qin, A.N.; Li, H.; Liu, X.; Qu, X.; Dai, K. Limitations of Gram staining for the diagnosis of infections following total hip or knee arthroplasty. *Exp. Ther. Med.* **2015**, *9*, 1857-1864.
29. Zahorec, R. Ratio of neutrophil to lymphocyte counts. Rapid and simple parameter of systemic inflammation and stress in critically ill. *Bratisl. Lek. Listy* **2001**, *102*, 5–14.
30. Hu, B.; Yang, X.R.; Xu, Y.; Sun, Y.F.; Sun, C.; Guo, W.; Zhang, X.; Wang, W.M.; Qiu, S.J.; Zhou, J.; et al. Systemic immune-inflammation index predicts prognosis of patients after curative resection for hepatocellular carcinoma. *Clin. Cancer Res.* **2014**, *20*, 6212–6222.

Disclaimer/Publisher's Note: The statements, opinions and data contained in all publications are solely those of the individual author(s) and contributor(s) and not of MDPI and/or the editor(s). MDPI and/or the editor(s) disclaim responsibility for any injury to people or property resulting from any ideas, methods, instructions or products referred to in the content.